International Journal of Coal Science & Technology (2024) 11:80
https://doi.org/10.1007/s40789-024-00734-5

RESEARCH

Mechanism and prevention of coal bursts in gob-side roadway floor under thick and hard roof in the deep mining area of Ordos

Jinlong Zhou[1,2,3] · Junfeng Pan[2] · Yongxue Xia[2] · Taotao Du[2] · Wengang Liu[4] · Chenyang Zhang[1,2]

Received: 2 January 2024 / Revised: 24 April 2024 / Accepted: 10 September 2024

Abstract

The complex stress environment in deep roadways, often exacerbated by thick and hard strata, frequently precipitates coal bursts, posing significant safety hazards. This paper investigates the mechanisms and preventive methods for coal bursts in the gob-side roadway floor (GSRF) under thick and hard roof in the Ordos region, China. First, the stress-distributing characters of GSRF were analyzed then a stress calculation formula was derived. A mechanical model was developed to determine the critical stress for buckling failure of the roadway floor strata. Criteria for the bursting instability of GSRF were then established. The lateral static load from the adjacent gob, the advancing static load from the working face, and the disturbance load from overlying thick and hard roof fractures combine to transmit high loads and energy to the roadway floor via the "roof → rib → floor" pathway, causing increased stress concentration and energy accumulation. When the conditions satisfy the criteria for bursting instability, coal bursts can occur on the roadway floor. To mitigate dynamic load disturbances, the paper proposes roof regional fracturing and abrasive water jet axial roof cutting. Hydraulic reaming of gutters in the roadway ribs and deep hole blasting at the roadway bottom corners are offered to alleviate the static loads on the surrounding rock. The implementation of targeted prevention measures for dynamic and static loads effectively reduces coal bursts in GSRF. These findings offer an example of preventing and controlling coal bursts in other mines of the Ordos region with comparable geological conditions.

Keywords Deep coal mining · Thick and hard roof · Gob-side roadway · Coal burst · Dynamic and static loads · Instability criteria

1 Introduction

China's energy source relies mainly on coal, making up roughly 55.3% of the country's total energy consumption. As the main coal supply base of China, the western region produces about 60.5% of the nation's total coal output (China National Coal Association. 2024). In the past few years, coal mining has been steadily expanding to deeper areas caused of the widespread and intensive coal exploitation in this region. For example, some new coal mines at Ordos, Inner Mongolia, have reached mining depths of 600–750 m (Zhao et al. 2023). The working faces in this area are characterized by significant depth, height, and width, coupled with rapid extraction rates, and are overlaid by multiple thick and hard strata. These conditions create a complex stress environment during deep and high-intensity mining, leading to frequent coal bursts in the advanced section of the gob-side roadway floor (GSRF) through the mining of the gob-side working face (GSWF), posing a severe risk to miners and constrains the secure and efficient extraction of coal resources. Therefore, it is critical to investigate the mechanisms and preventive methods of coal bursts in GSRF under such mining conditions. The findings of this research will provide essential guidance for preventing coal bursts in GSRF, promoting the safe and efficient operation of coal mines.

Coal seam mining induces stress field redistribution, affecting stress distribution in roadways and adjacent

✉ Jinlong Zhou
zhoujlcumtb@163.com

1 China Coal Research Institute, Beijing 100013, China

2 CCTEG Coal Mining Research Institute, Beijing 100013, China

3 School of Energy and Mining Engineering, China University of Mining and Technology (Beijing), Beijing 100083, China

4 Research Institute of Emergency Science, China Coal Research Institute, Beijing 100013, China

working face floors, potentially leading to roadway floor damage and coal bursts. Global research efforts have examined stress calculation and distribution characteristics in roadways and gob floors. Yang et al. (2020) established a mechanical model for roadway floors affected by mining activities, demonstrating asymmetric stress distribution and establishing criteria for layered floor failure. Liu et al. (2022) analyzed stress distribution patterns in working face floors, analyzing characteristics of sectional floor damage. They concluded that the asymmetric roadway floor damage is attributed to contrasting failure modes in rock masses on either side of the roadway. Shan et al. (2021, 2022) constructed a model to calculate the lateral abutment pressure of gob floors, providing stress deviation distribution characteristics, analyzing influencing factors, and revealing the gob floor's plastic failure mechanism. Additionally, Suchowerska et al. (2013, 2014) simulated vertical and horizontal stresses in floors and derived stress distribution patterns.

Early coal burst mechanism theories, including strength theory (Cook 1965), stiffness theory (Wawersik et al. 1970; Hudson et al. 1972; Linkov 1996), energy theory (Cook et al. 1966), and bursting liability theory (Bieniawski 1967) were primarily developed by scholars from Germany, Poland, and the Soviet Union. Building upon these foundational theories, Chinese researchers have conducted systematic and in-depth studies, resulting in the development of several new theories. These include the "three criteria" theory (Li 1985), the "three factors" theory (Qi et al. 1995), the dynamic and static loads superposition-induced burst theory (Dou et al. 2014; Li et al. 2015; He et al. 2017), the strength weakening and reduction burst theory (Dou et al. 2005), the disturbance response instability theory (Pan 2018; Pan et al. 2023), the creep instability theory, the burst start-up theory (Pan et al. 2012), and the butterfly-shaped burst mechanism of roadways (Zhao et al. 2016). These mechanisms greatly enhance comprehension of the coal burst process. However, research on the coal burst mechanism in roadway floors remains limited. Studies predominantly use numerical simulation methods to simulate stress and energy distribution laws on roadway floors. These simulations facilitate the analysis and revelation of floor strata stability and the influencing factors of coal bursts in the floor (Dong et al. 2021; Guo et al. 2021). Additionally, investigations explore the influence of various factors on coal bursts in the floor (Mu et al. 2019).

Scholars have not only investigated coal burst mechanisms but also systematically studied prevention and control theories and methods for deposit conditions with thick and hard roof. Hydraulic fracturing technology is utilized for low-position thick and hard roof pressure relief, thereby reducing the disturbance to the surrounding rock in roadways caused by roof rupture, thus preventing coal bursts (Fan et al. 2012; He et al. 2012; Huang et al. 2018; Zhang et al. 2022). Roof regional fracturing is applied to weaken the middle and high-position thick and hard strata, altering their properties, diminishing the dynamic load from roof fracture, and easing the intensity of strata behavior in stopes (Yu et al. 2019; Gao et al. 2021; Kang et al. 2022; Pan et al. 2022a). Furthermore, deep hole blasting serves as a pre-splitting technique to induce destressing (Ma et al. 2023; Wu et al. 2023), while directional tension blasting technology induces directional slicing destressing to reduce elastic energy accumulation and mitigate dynamic load disturbance from energy release in thick and hard roof conditions (Zhang et al. 2020; Wang et al. 2023a; Yang et al. 2023). For roadway support to prevent coal bursts, hydraulic supports equipped with energy absorption devices are implemented to reinforce roadway supports, absorb the energy from deformation and damage to roadways, and reduce dynamic load disturbances (Pan et al. 2020; Guo et al. 2023; Tang et al. 2023). High-load, large-deformation bolts, and energy-absorbing bolts are concurrently utilized to reinforce surrounding rocks of roadways. These bolts effectively manage surrounding rocks deformation and absorb energy from dynamic load induced by roof fracture (Wang et al. 2022b, 2023b; Lou et al. 2023; Zhou et al. 2023), thereby mitigating dynamic load resulting from thick and hard roof fracture (Wang et al. 2022a). High-impact toughness bolts strengthen the support system by enhancing its strength and energy absorption capacity. The coordinated deformation of the support structure with the surrounding rock facilitates energy absorption, thereby increasing the support system's resistance to impact and reinforcing the stability of the roadway surrounding rocks (Fu et al. 2019; Kang et al. 2020).

Current research endeavors have provided valuable insights into stress distribution characteristics in roadway floors, mechanisms of coal bursts, and effective prevention and control strategies for coal bursts in thick and hard roof conditions. However, research on the mechanism and prevention methods of coal bursts in GSRF under thick and hard roof conditions in the deep mining area of Ordos remains limited. Addressing this problem, this study first analyzes the stress distribution in GSRF to determine its characteristics. Then, based on the strata fracture characteristics when the coal bursts in the floor occur on-site, a mechanical model of beam-buckling failure of floor strata was established to obtain the critical stress for floor strata failure. Based on this, a criterion for the bursting instability of GSRF was proposed, revealing the mechanism of coal bursts in GSRF. Drawing upon the mechanism of coal bursts in GSRF, preventive and control measures for coal bursts were proposed. The study provides valuable insights for preventing and controlling coal bursts in GSRF under thick and hard roof conditions in the Ordos region.

2 Description of the study site

Over the past few years, several large coal mines have been built in the Ordos region of China. Due to the deep burial depth (600–750 m) and the influence of thick and hard strata above the working face, these mines frequently experience coal bursts in GSRF. This phenomenon significantly affects the safe and efficient production of coal mines. This study presents a case study of the Hongqinghe Coal Mine in Xinjie of Ordos to investigate the mechanism and prevention of coal bursts in GSRF. The study aims to offer guidance for the prevention and control of coal bursts in similar geological conditions in the region.

The Hongqinghe Coal Mine boasts a designed production capacity of 15 Mt/a. It employs the vertical shaft development method, primarily extracting from the 3^{-1} coal seam. The $3^{-1}101$ working face resides in the southern division of the mine. The $3^{-1}103$ working face, a continuation of the $3^{-1}101$ working face, has an average depth of 707.15 m, a width of 210 m, and an advancing length of 2480 m. The coal seam thickness varies from 5.52 to 7.20 m, averaging at 6.36 m. Employing a fully mechanized mining method, the advance speed of the working face is about 8 m/d. Three roadways accompany the working face: the $3^{-1}101$ material roadway, the $3^{-1}103$ belt roadway, and the $3^{-1}103$ material roadway. During the extraction process of the $3^{-1}101$ working face, significant impact deformation occurred in the original material roadway, which negatively impacted production. A new material roadway for the $3^{-1}101$ working face was constructed, positioned 30 m from the previous one.

During the mining process of the $3^{-1}103$ working face, the $3^{-1}101$ material roadway (gob-side roadway (GSR)) frequently experiences coal bursts. The primary characteristics include sudden cracking and bulging of the floor, subsidence of the roof, and collapse of ribs, and bolts fracture. The occurrence of coal bursts significantly compromised the safety and production of the working face, emerging as a major obstacle to the safe and efficient excavation of the Hongqinghe Coal Mine. The layout of the $3^{-1}101$, and $3^{-1}103$ working faces and typical bursting failure characteristics of GSR are shown in Fig. 1.

In the Hongqinghe Coal Mine, coal bursts occurring on the GSR result in substantial bursting failure of the roadway floor, a typical manifestation of coal bursts in the deep mining area of Ordos. Previous research has demonstrated a strong correlation between the occurrence of coal bursts and stress concentration and energy accumulation within the coal-rock mass (Gong et al. 2022; He et al. 2023). Coal

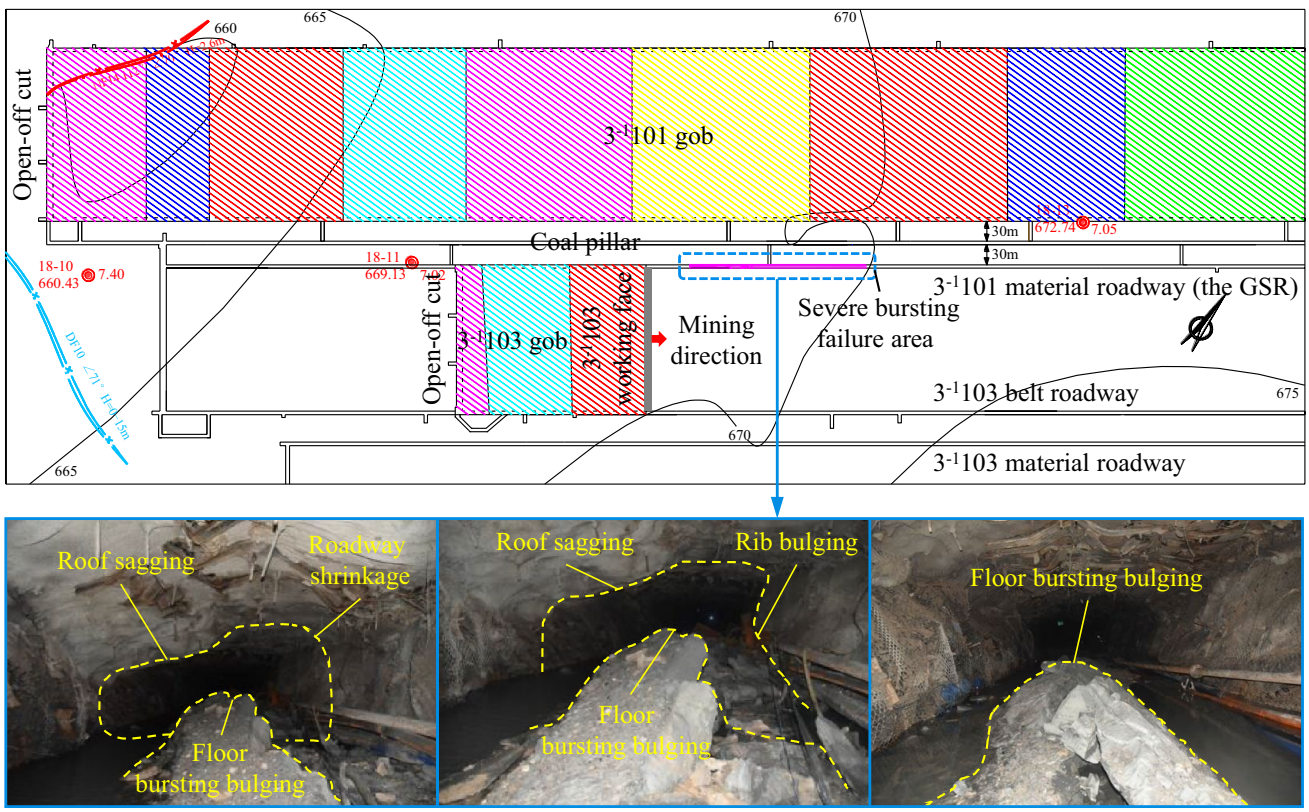

Fig. 1 The layout of the $3^{-1}101$, and $3^{-1}103$ working faces and typical bursting failure characteristics of GSR

bursts in GSRF are closely related to the stress and energy exerted on the roadway surrounding rock, especially the stress distribution status of GSRF. Thus, this article first analyzes the stress distribution of GSRF and obtains its characteristics. Then, using the strata fracture characteristics when the coal bursts in the floor occur on-site, a mechanical model of buckling failure of the roadway floor strata was established, and the stability of roadway floor strata was analyzed, thereby determining the critical stress required for the floor strata to fracture. Based on this, a criterion for the bursting instability of GSRF was proposed, and the mechanism of coal bursts in GSRF was revealed. Finally, the preventive measures for coal bursts in GSRF were proposed.

3 Stress analysis of GSRF

The GSR is subjected to the transfer load from the adjacent gob roof and the mining activities at the working face, resulting in high stress and energy generation. This stress and energy subsequently propagate to the roadway floor through the roadway ribs, potentially causing high-stress concentration and energy accumulation within the floor strata. However, the GSRF, typically in an exposed state or with only simple support, is susceptible to instability due to sudden increases in stress or dynamic load disturbances. The coal bursts in roadway floors arise when the floor strata exhibit bursting liability. The stability of the floor strata significantly influences not only the occurrence of coal bursts in roadway floors but also the overall roadway. Consequently, an analysis of the stress state of GSRF becomes imperative.

3.1 Stress distribution characteristics of floor in GSWF

The excavation of underground roadways and mining of working faces during coal extraction induce stress redistribution in the surrounding rock, forming the mining-induced stress field. This, in combination with the in-situ stress field and the stress field generated by the support system, creates a complex stress environment in the coal mine (Kang 2008). According to Zhao et al. (2023), the GSR is primarily subjected to lateral static load stress from the adjacent gob, advanced abutment pressure from the mining of the working face, and dynamic load disturbances caused by the fracture of overlying thick and hard strata. These dynamic and static loads are transmitted to the roadway floor via the "roof → rib → floor" pathway, influencing the stress of the roadway floor. Therefore, the stress distribution characteristics of the floor in the GSWF significantly affect the stress state of the floor. This section primarily analyzes the stress distribution of the floor in GSWF under mining-induced static load. Based on the mine pressure theory (Qian et al. 2010), the vertical stress distribution of the floor in front of GSWF is shown in Fig. 2.

According to Fig. 2, the vertical stress distribution of floor can be divided into following sections from the gob to the solid coal in front of GSWF: (1) the in-situ stress zone in gob side (with the in-situ stress as γH); (2) the stress recovery zone in gob (with the stress gradually increasing and approaching the in-situ stress value); (3) the stress reduction zone in gob side of coal pillar; (4) the stress increase zone in coal pillar floor caused by the adjacent gob and the GSR (with the stress higher than the in-situ stress and asymmetric distribution, with peak stresses of $K_1\gamma H$ and $K_2\gamma H$); (5) the stress reduction zone in roadway side of coal pillar; (6) the unloading zone of GSRF; (7) the stress reduction zone in roadway side of solid coal; (8) the stress increase zone in solid coal, the range where the vertical stress of the floor

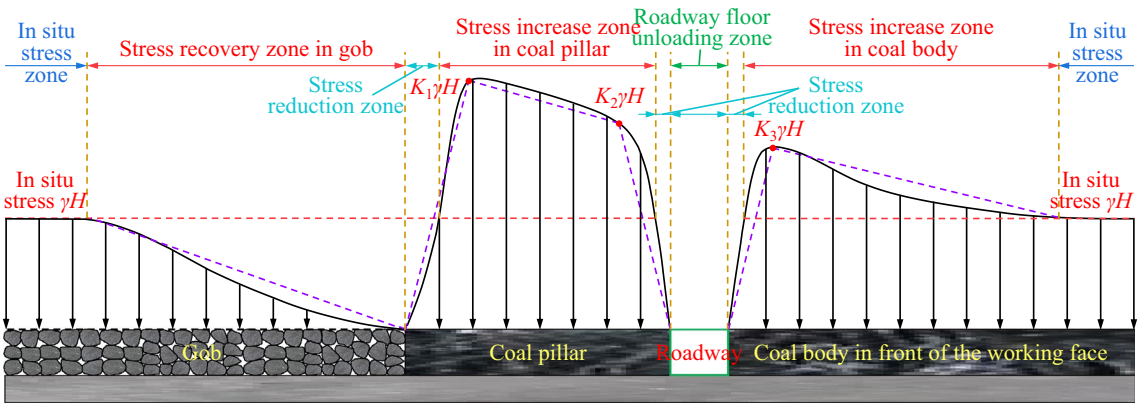

Fig. 2 Schematic diagram of vertical stress distribution of floor in front of GSWF under the mining influence

exceeds the in-situ stress in the solid coal region (with a peak stress of $K_3\gamma H$), and (9) the in-situ stress zone in solid coal, beyond stress increase zone and away from the GSR, the stress distribution in the floor transitions to the in-situ stress. To simplify the calculation of floor stress in Sect. 3.2, the vertical stress distribution curve of the floor is approximated by a linearization, as illustrated by the purple dashed line in Fig. 2.

3.2 Stress analysis of the roadway floor

In the deep mining area of Ordos, coal bursts in floors mainly occur in the advanced working face zone of GSR. Therefore, in this section, we analyze the stress state of the roadway floor in the advanced working face of GSR to lay the foundation for revealing the mechanism of coal bursts in GSRF.

Based on the stress superposition principle, the stress at any point in the roadway floor can be decomposed into the in-situ stress and the additional stress caused by the vertical stress increment of the floor (Hua 1983). The in-situ stress at a specific location within the roadway floor strata is determined by its distance from the surface. Consequently, the process of determining the stress at any given point within the roadway floor strata can be simplified to calculate the additional stress induced by the vertical stress increment at that point. With the coal pillar side of GSR, as the origin O, the x-axis parallel to the floor pointing to the right, and the y-axis perpendicular to the floor pointing downward, a model is established for calculating the vertical stress increment and the additional stress of the floor in the advanced section of GSWF, as shown in Fig. 3.

Based on Fig. 3, the linear load expressions for each segment are:

$$\begin{cases} q_1(x) = a_1x + b_1 = \frac{-\gamma H}{L_1}\left(x + L_1 + L_2 + L_3 + L_4\right) & \left(-L_1 - L_2 - L_3 - L_4 \le x \le -L_2 - L_3 - L_4\right) \\ q_2(x) = a_2x + b_2 = \frac{K_1\gamma H}{L_2}\left(x + L_2 + L_3 + L_4\right) - \gamma H & \left(-L_2 - L_3 - L_4 \le x \le -L_3 - L_4\right) \\ q_3(x) = a_3x + b_3 = \frac{(K_2 - K_1)\gamma H}{L_3}\left(x + L_3 + L_4\right) + \left(K_1 - 1\right)\gamma H & \left(-L_3 - L_4 \le x \le -L_4\right) \\ q_4(x) = a_4x + b_4 = \frac{-K_2\gamma H}{L_4}x - \gamma H & \left(-L_4 \le x \le 0\right) \\ q_5(x) = a_5x + b_5 = -\gamma H & \left(0 \le x \le L_5\right) \\ q_6(x) = a_6x + b_6 = \frac{K_3\gamma H}{L_6}\left(x - L_5\right) - \gamma H & \left(L_5 \le x \le L_5 + L_6\right) \\ q_7(x) = a_7x + b_7 = \frac{(1 - K_3)\gamma H}{L_7}\left(x - L_5 - L_6 - L_7\right) & \left(L_5 + L_6 \le x \le L_5 + L_6 + L_7\right) \end{cases} \tag{1}$$

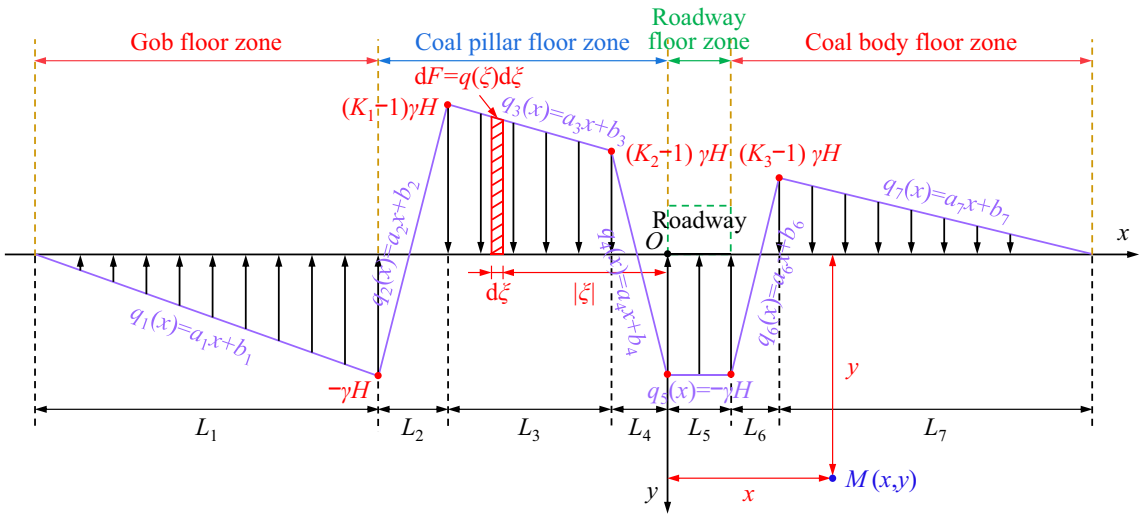

Fig. 3 Calculation model of vertical stress increment and additional stress of floor

where $q_i(x)$ ($i=1$–7) is the function of the i-th segment linear load, γ is the average bulk density of the overlying strata, H is the burial depth of the coal seam, L_i ($i=1$–7) is the distribution length of the i-th segment linear load in the x-axis direction, and K_i ($i=1$–3) are the stress concentration coefficients of the gob side of coal pillar, the roadway side of coal pillar, and the roadway side of solid coal.

Based on the solution methods in elasticity mechanics for calculating the stress at a point caused by a distributed force on the boundary of a half-plane body, we can calculate the additional stress produced by the vertical stress increment at any given point in the floor (Xu 2018). Assuming a small length $d\xi$ at a distance ξ from the origin O, the corresponding force $dF=q(\xi)d\xi$ can be defined as a minor concentrated force. The stress caused by the minor concentrated force $dF=q(\xi)d\xi$ at any point M (x, y) in the floor is given by:

$$\begin{cases} d\sigma_x = \dfrac{2q(\xi)}{\pi}\dfrac{(x-\xi)^2 y}{\left[(x-\xi)^2+y^2\right]^2}d\xi \\ d\sigma_y = \dfrac{2q(\xi)}{\pi}\dfrac{y^3}{\left[(x-\xi)^2+y^2\right]^2}d\xi \\ d\tau_{xy} = \dfrac{2q(\xi)}{\pi}\dfrac{(x-\xi)y^2}{\left[(x-\xi)^2+y^2\right]^2}d\xi \end{cases} \tag{2}$$

where σ_x, σ_y, and τ_{xy} are the horizontal stress, vertical stress, and shear stress at point M (x, y), and $q(\xi)$ is the load value at point (ξ, y).

By integrating Eq. (2) over the interval [$-L_1$-L_2-L_3-L_4, $-L_2$-L_3-L_4], the additional stresses $\Delta\sigma_{x1}$, $\Delta\sigma_{y1}$, and $\Delta\tau_{xy1}$ caused by the linear load $q_1(x)$ at any point M (x, y) in the floor can be calculated using Eq. (3).

$$\begin{cases} \Delta\sigma_{x1} = \displaystyle\int_{-L_1-L_2-L_3-L_4}^{-L_2-L_3-L_4} d\sigma_x = \frac{2}{\pi}\int_{-L_1-L_2-L_3-L_4}^{-L_2-L_3-L_4} \frac{q_1(\xi)(x-\xi)^2 y}{\left[(x-\xi)^2+y^2\right]^2}d\xi \\ \Delta\sigma_{y1} = \displaystyle\int_{-L_1-L_2-L_3-L_4}^{-L_2-L_3-L_4} d\sigma_y = \frac{2}{\pi}\int_{-L_1-L_2-L_3-L_4}^{-L_2-L_3-L_4} \frac{q_1(\xi)y^3}{\left[(x-\xi)^2+y^2\right]^2}d\xi \\ \Delta\tau_{xy1} = \displaystyle\int_{-L_1-L_2-L_3-L_4}^{-L_2-L_3-L_4} d\tau_{xy} = \frac{2}{\pi}\int_{-L_1-L_2-L_3-L_4}^{-L_2-L_3-L_4} \frac{q_1(\xi)(x-\xi)y^2}{\left[(x-\xi)^2+y^2\right]^2}d\xi \end{cases} \tag{3}$$

where $\Delta\sigma_{x1}$, $\Delta\sigma_{y1}$, and $\Delta\tau_{xy1}$ are the additional horizontal stress, additional vertical stress, and additional shear stress caused by the linear load $q_1(x)$ at any point M (x, y) in the floor.

Using the same method, the additional stresses $\Delta\sigma_{xi}$, $\Delta\sigma_{yi}$, $\Delta\tau_{xyi}$ ($i=2$–7) caused by the linear loads $q_i(x)$ ($i=2$–7) at any point M (x, y) in the floor can be calculated. According to the superposition principle (Hua 1983), the stress at any point M (x, y) in the floor can be obtained by superimposing the additional stresses caused by the linear loads $q_i(x)$ ($i=1$–7) and the in-situ stress. Therefore, the stress expression at any point M (x, y) in the floor is:

$$\begin{cases} \sigma_x = \displaystyle\sum_{i=1}^{7}\Delta\sigma_{xi} + \lambda\gamma(H+y) \\ \sigma_y = \displaystyle\sum_{i=1}^{7}\Delta\sigma_{yi} + \gamma(H+y) \\ \tau_{xy} = \displaystyle\sum_{i=1}^{7}\Delta\tau_{xyi} \end{cases} \tag{4}$$

where λ is the lateral pressure coefficient, which is generally taken as 1.2.

In this section, we mainly study the stability of the floor strata under horizontal squeezing stress. Therefore, we only calculate the additional horizontal stress caused by the linear loads $q_i(x)$ ($i=1$–7) at any point M (x, y) in the floor.

$$\begin{aligned} \Delta\sigma_{x1} &= \int_{-L_1-L_2-L_3-L_4}^{-L_2-L_3-L_4} d\sigma_x = \frac{2}{\pi}\int_{-L_1-L_2-L_3-L_4}^{-L_2-L_3-L_4} \frac{q_1(\xi)(x-\xi)^2 y}{\left[(x-\xi)^2+y^2\right]^2}d\xi \\ &= \frac{2}{\pi}\int_{-L_1-L_2-L_3-L_4}^{-L_2-L_3-L_4} \frac{\frac{-\gamma H}{L_1}\left(\xi+L_1+L_2+L_3+L_4\right)(x-\xi)^2 y}{\left[(x-\xi)^2+y^2\right]^2}d\xi \\ &= \left\{ \begin{array}{l} \dfrac{\gamma H\left(x+L_1+L_2+L_3+L_4\right)}{\pi L_1}\arctan\left(\dfrac{x-\xi}{y}\right) - \dfrac{\gamma H y}{\pi L_1}\ln\left[(x-\xi)^2+y^2\right] - \\ \dfrac{\gamma H\left(L_1+L_2+L_3+L_4\right)(x-\xi)+\gamma H\left(x^2+y^2-\xi x\right)}{\pi L_1\left[(x-\xi)^2+y^2\right]}y \end{array} \right\}\Bigg|_{\xi=-L_1-L_2-L_3-L_4}^{\xi=-L_2-L_3-L_4} \end{aligned} \tag{5}$$

$$\Delta\sigma_{x2}=\int_{-L_2-L_3-L_4}^{-L_3-L_4}\mathrm{d}\sigma_x=\frac{2}{\pi}\int_{-L_2-L_3-L_4}^{-L_3-L_4}\frac{q_2(\xi)(x-\xi)^2y}{\left[(x-\xi)^2+y^2\right]^2}\mathrm{d}\xi$$
$$=\frac{2}{\pi}\int_{-L_2-L_3-L_4}^{-L_3-L_4}\frac{\left[\frac{K_1\gamma H}{L_2}\left(\xi+L_2+L_3+L_4\right)-\gamma H\right](x-\xi)^2y}{\left[(x-\xi)^2+y^2\right]^2}\mathrm{d}\xi$$
$$=\left\{\begin{array}{l}\frac{-\frac{K_1\gamma H}{L_2}\left(x+L_2+L_3+L_4\right)+\gamma H}{\pi}\arctan\left(\frac{x-\xi}{y}\right)+\frac{K_1\gamma Hy}{\pi L_2}\ln\left[(x-\xi)^2+y^2\right]+\\ \frac{\left[\frac{K_1\gamma H}{L_2}\left(L_2+L_3+L_4\right)-\gamma H\right](x-\xi)+\frac{K_1\gamma H}{L_2}\left(x^2+y^2-\xi x\right)}{\pi\left[(x-\xi)^2+y^2\right]}y\end{array}\right\}\Bigg|_{\xi=-L_2-L_3-L_4}^{\xi=-L_3-L_4}\tag{6}$$

$$\Delta\sigma_{x3}=\int_{-L_3-L_4}^{-L_4}\mathrm{d}\sigma_x=\frac{2}{\pi}\int_{-L_3-L_4}^{-L_4}\frac{q_3(\xi)(x-\xi)^2y}{\left[(x-\xi)^2+y^2\right]^2}\mathrm{d}\xi$$
$$=\frac{2}{\pi}\int_{-L_3-L_4}^{-L_4}\frac{\left[\frac{(K_2-K_1)\gamma H}{L_3}\left(\xi+L_3+L_4\right)+\left(K_1-1\right)\gamma H\right](x-\xi)^2y}{\left[(x-\xi)^2+y^2\right]^2}\mathrm{d}\xi$$
$$=\left\{\begin{array}{l}-\frac{\frac{(K_2-K_1)\gamma H}{L_3}\left(x+L_3+L_4\right)+\left(K_1-1\right)\gamma H}{\pi}\arctan\left(\frac{x-\xi}{y}\right)+\frac{\left(K_2-K_1\right)\gamma Hy}{\pi L_3}\ln\left[(x-\xi)^2+y^2\right]+\\ \frac{\left[\frac{(K_2-K_1)\gamma H}{L_3}\left(L_3+L_4\right)+\left(K_1-1\right)\gamma H\right](x-\xi)+\frac{(K_2-K_1)\gamma H}{L_3}\left(x^2+y^2-\xi x\right)}{\pi\left[(x-\xi)^2+y^2\right]}y\end{array}\right\}\Bigg|_{\xi=-L_3-L_4}^{\xi=-L_4}\tag{7}$$

$$\Delta\sigma_{x4}=\int_{-L_4}^{0}\mathrm{d}\sigma_x=\frac{2}{\pi}\int_{-L_4}^{0}\frac{q_4(\xi)(x-\xi)^2y}{\left[(x-\xi)^2+y^2\right]^2}\mathrm{d}\xi=\frac{2}{\pi}\int_{-L_4}^{0}\frac{\left(\frac{-K_2\gamma H}{L_4}\xi-\gamma H\right)(x-\xi)^2y}{\left[(x-\xi)^2+y^2\right]^2}\mathrm{d}\xi$$
$$=\left\{\begin{array}{l}\frac{\frac{K_2\gamma H}{L_4}x+\gamma H}{\pi}\arctan\left(\frac{x-\xi}{y}\right)-\frac{K_2\gamma Hy}{\pi L_4}\ln\left[(x-\xi)^2+y^2\right]-\\ \frac{\gamma H(x-\xi)+\frac{K_2\gamma H}{L_4}\left(x^2+y^2-\xi x\right)}{\pi\left[(x-\xi)^2+y^2\right]}y\end{array}\right\}\Bigg|_{\xi=-L_4}^{\xi=0}\tag{8}$$

$$\Delta\sigma_{x5}=\int_{0}^{L_5}\mathrm{d}\sigma_x=\frac{2}{\pi}\int_{0}^{L_5}\frac{q_5(\xi)(x-\xi)^2y}{\left[(x-\xi)^2+y^2\right]^2}\mathrm{d}\xi=\frac{2}{\pi}\int_{0}^{L_5}\frac{-\gamma H(x-\xi)^2y}{\left[(x-\xi)^2+y^2\right]^2}\mathrm{d}\xi$$
$$=\frac{\gamma H}{\pi}\left[\arctan\left(\frac{x-\xi}{y}\right)-\frac{(x-\xi)y}{(x-\xi)^2+y^2}\right]\Bigg|_{\xi=0}^{\xi=L_5}\tag{9}$$

$$\Delta\sigma_{x6}=\int_{L_5}^{L_6}\mathrm{d}\sigma_x=\frac{2}{\pi}\int_{L_5}^{L_6}\frac{q_6(\xi)(x-\xi)^2y}{\left[(x-\xi)^2+y^2\right]^2}\mathrm{d}\xi=\frac{2}{\pi}\int_{L_5}^{L_6}\frac{\left[\frac{K_3\gamma H}{L_6}(\xi-L_5)-\gamma H\right](x-\xi)^2y}{\left[(x-\xi)^2+y^2\right]^2}\mathrm{d}\xi$$
$$=\left\{\begin{array}{l}\dfrac{-\frac{K_3\gamma H}{L_6}(x-L_5)+\gamma H}{\pi}\arctan\left(\dfrac{x-\xi}{y}\right)+\dfrac{K_3\gamma Hy}{\pi L_6}\ln\left[(x-\xi)^2+y^2\right]+\\ \dfrac{-\left(\frac{K_3\gamma H}{L_6}L_5+\gamma H\right)(x-\xi)+\frac{K_3\gamma H}{L_6}\left(x^2+y^2-\xi x\right)}{\pi\left[(x-\xi)^2+y^2\right]}y\end{array}\right\}\Bigg|_{\xi=L_5}^{\xi=L_6} \tag{10}$$

$$\Delta\sigma_{x7}=\int_{L_6}^{L_7}\mathrm{d}\sigma_x=\frac{2}{\pi}\int_{L_6}^{L_7}\frac{q_7(\xi)(x-\xi)^2y}{\left[(x-\xi)^2+y^2\right]^2}\mathrm{d}\xi$$
$$=\frac{2}{\pi}\int_{L_6}^{L_7}\frac{\left[\frac{(1-K_3)\gamma H}{L_7}(\xi-L_5-L_6-L_7)\right](x-\xi)^2y}{\left[(x-\xi)^2+y^2\right]^2}\mathrm{d}\xi$$
$$=\left\{\begin{array}{l}\dfrac{(K_3-1)\gamma H(x-L_5-L_6-L_7)}{\pi L_7}\arctan\left(\dfrac{x-\xi}{y}\right)+\dfrac{(1-K_3)\gamma Hy}{\pi L_7}\ln\left[(x-\xi)^2+y^2\right]+\\ \dfrac{(K_3-1)\gamma H(L_5+L_6+L_7)(x-\xi)+(1-K_3)\gamma H(x^2+y^2-\xi x)}{\pi L_7\left[(x-\xi)^2+y^2\right]}y\end{array}\right\}\Bigg|_{\xi=L_6}^{\xi=L_7} \tag{11}$$

By substituting Eqs. (5) to (11) into Eq. (4), the horizontal stress σ_x at any point M (x, y) in the floor under the mining influence can be obtained.

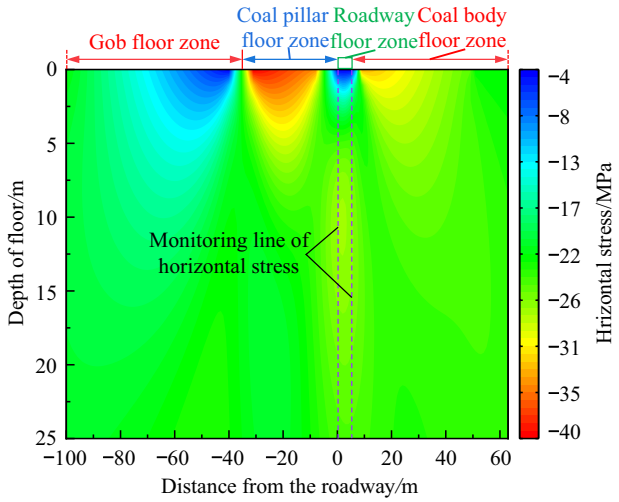

Fig. 4 Distribution of horizontal stress of the floor at different depths

3.3 Distribution of horizontal stress in roadway floor

In order to verify the reliability of the calculation method of horizontal stress in GSWF was proposed in Sect. 3.2, and also to provide a reference for the stability analysis of roadway floor strata. The calculation of the distribution law of horizontal stress on the roadway floor was carried out with Hongqinghe Coal Mine as the engineering background. Considering the geological data, field measurements, and numerical simulation results of the Hongqinghe Coal Mine, the following parameters are taken into account: the average burial depth H of the 3^{-1} coal seam is 730 m, the average bulk density γ of the overlying strata is 25 kN/m^3, the lateral pressure coefficient λ is 1.2, the stress concentration coefficients K_i $(i=1–3)$ are 2.0, 1.7, and 1.6, and the widths of the linear loads L_i $(i=1–7)$ are 60, 9, 23, 8, 5, 8, and 50 m. By substituting these parameters into Eq. (4), the horizontal stress σ_x at any point M (x, y) in GSRF can be calculated. The distribution of horizontal stress of the floor at different depths under mining influence can be obtained using MATLAB software, as shown in Fig. 4.

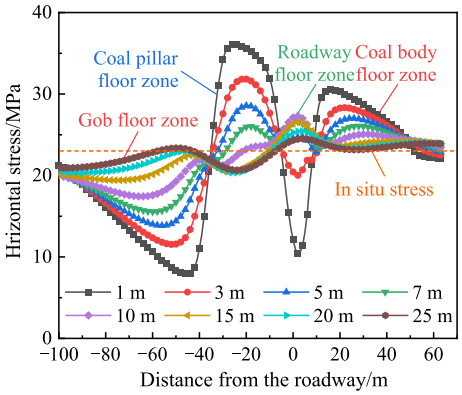

Fig. 5 Variation of horizontal stress of the floor in different zones and floor depths

Figure 4 demonstrates that the excavation of the roadway and the mining of the working face cause a redistribution of horizontal stress in the floor. The gob and GSRF experience a significant reduction in horizontal stress, with a reduction rate of approximately 74.89%. Conversely, the sides of the coal pillar and solid coal exhibit a significant increase in horizontal stress, with growth rates of approximately 73.52% and 48.86%, respectively. The horizontal stress in each region increases or decreases accordingly with increasing floor depth. As the floor depth approaches 25 m, the horizontal stress in the floor becomes approximately uniformly distributed and tends to a constant value.

The horizontal stress of the floor, particularly in the GSRF, significantly influences the stability of the floor strata and the occurrence of floor bursts. Horizontal stress variations in floor strata under mining disturbance calculated using the proposed method (Sect. 3.2) elucidate stress distributions in different zones and floor depths, as shown in Fig. 5.

Figure 5 demonstrates substantial horizontal stress variations across distinct floor zones as floor depth increases. These variations include phenomena of horizontal stress unloading and stress concentration. For this study, the stress unloading coefficient is defined as the ratio of the difference between the in-situ stress and the actual stress to the in-situ stress. In the gob, the floor experiences stress unloading within a certain depth range, and the stress unloading coefficient exhibits a decreasing trend from 0.64 to 0.04 with increasing floor depth. At a floor depth of 25 m, the horizontal stress within the gob floor progressively converges towards the in-situ stress state. Within the coal pillar floor, the horizontal stress undergoes stress concentration, exhibiting a gradual approach towards the in-situ stress state as the floor depth increases. As the floor depth increases, the stress concentration coefficient exhibits a decreasing trend, transitioning from 1.65 to 1.10. Beyond a floor depth of 10 m, the horizontal stress within the coal pillar floor progressively converges towards the in-situ stress state. Within a specific depth range, the horizontal stress within the solid coal undergoes a stress concentration phenomenon. With floor depth increases, the stress concentration coefficient exhibits a decreasing trend, transitioning from 1.39 to 1.06. At a floor depth of 25 m, the horizontal stress within the solid coal progressively

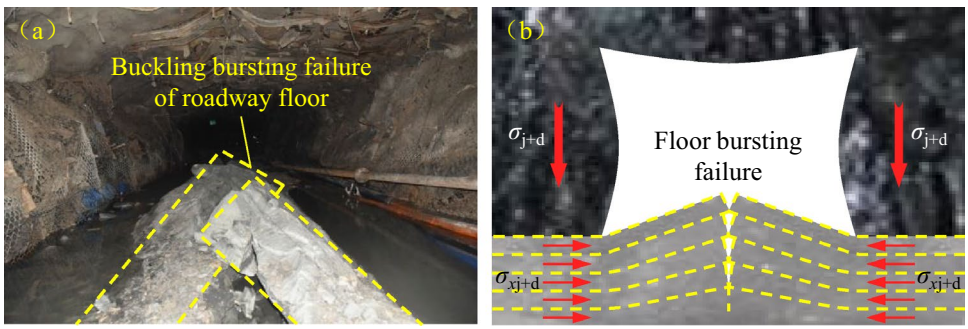

Fig. 6 Photos of bursting failure of roadway floor, and schematic diagram of buckling bursting failure of roadway floor: **a** Photos of bursting failure of roadway floor, **b** Schematic diagram of buckling bursting failure of roadway floor

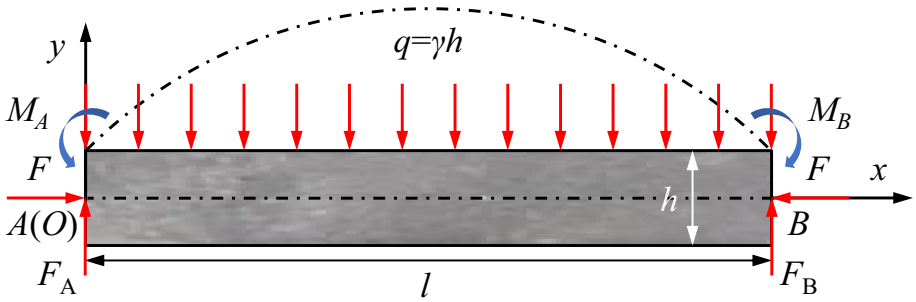

Fig. 7 Mechanical model of beam-buckling failure of roadway floor

converges toward the in-situ stress state. Conversely, the horizontal stress within the roadway floor experiences a transition from stress unloading to stress concentration with increasing floor depth. With a progressive increase in floor depth, the horizontal stress gradually converges towards the in-situ stress state. The peak stress unloading coefficient in the roadway floor reaches approximately 0.52, while the peak stress concentration coefficient attains a value of approximately 1.25.

4 Criteria and mechanism for the bursting instability of GSRF

4.1 Analysis of the mechanical behavior for buckling bursting failure in roadway floor

In underground coal mines, the strata exhibit a laminated distribution. When the roadway floor strata are subjected to high horizontal compressive stress, it undergoes delamination. This process initiates from the top and progressively bends and bulges into the roadway layer by layer. The rate of layer cracking decreases as the distance from the free surface of the floor increases. This continues until a certain layer of the floor strata no longer satisfies the conditions for bending failure, at which point the depth of the floor failure stops increasing. Within the strata of GSRF, if the strata exhibit high strength and strong bursting liability, it will accumulate a substantial amount of elastic energy under the influence of high horizontal stress. This accumulation may suddenly lead to the buckling bursting failure of the roadway floor under external dynamic load disturbances. The behavior characteristics of coal bursts in GSRF at the Hongqinghe Coal Mine, as shown in Fig. 6.

Upon the extraction of the coal seam, the elevated stress and energy within the surrounding rock of the roadway transmitted from the roof to the floor through the coal body in roadway ribs. Upon reaching its critical value for buckling failure, the horizontal stress exerted within the floor strata initiates floor buckling. This failure of the roadway floor provides space for the bulging of roadway bottom corners, which can potentially lead to failure of the roadway ribs, ultimately escalating to a severe roof fall hazard. Within the complex stress environment resulting from the combined influence of high static load and disturbance dynamic load in deep mining, the likelihood of a coal burst occurring in the roadway is elevated. Therefore, a comprehensive analysis of the stability characteristics of the roadway floor strata is of paramount importance.

In order to understand the instability and failure mechanism of the roadway floor strata, mechanical analysis of a specific layer of the roadway floor is conducted, considering the distribution characteristics of the strata in underground coal mines. Strictly speaking, for layered strata in roadways, the instability mechanism of the floor strata under horizontal compressive stress should be analyzed according to the instability theory of the plate. However, when the distance along the roadway axis is twice beyond the roadway width, the mechanical model can be simplified to a beam model. According to Cao et al. (2013), this study establishes a mechanical model for beam-buckling failure of the roadway floor, as shown in Fig. 7.

Figure 7 considers only the horizontal compressive stress and the self-weight stress exsert on the strata. According to the theory of mechanics of materials (Sun et al. 2009), the approximate differential equation for the deflection curve of the roadway floor strata is:

$$\frac{\mathrm{d}^2\omega}{\mathrm{d}x^2} = -\frac{M(x)}{EI} \tag{12}$$

where ω is the deflection of the roadway floor strata, $M(x)$ is the bending moment at the section x from the origin O, E is the elastic modulus of the roadway floor strata, and I is the moment of inertia of the roadway floor strata.

From the equilibrium state of the roadway floor strata, it is known that $\sum M = 0$, which means:

$$M(x) + F_{\mathrm{A}}x - M_A - \frac{1}{2}qx^2 - F\omega = 0 \tag{13}$$

where F_{A} is the support reaction at point A, M_{A} is the bending moment at point A, q is the uniformly distributed load formed by the self-weight of the roadway floor strata, and F is the horizontal compressive stress exerted on the roadway floor strata.

From Eq. (13), it can be derived that:

$$M(x) = M_A - F_{\mathrm{A}}x + \frac{1}{2}qx^2 + F\omega = \frac{q}{2}\left(x^2 - lx + \frac{l^2}{6}\right) + F\omega \tag{14}$$

where l is the width of the roadway.

Substituting Eq. (14) into Eq. (12):

$$\frac{\mathrm{d}^2\omega}{\mathrm{d}x^2} = -\frac{q}{2EI}\left(x^2 - lx + \frac{l^2}{6}\right) + \frac{F\omega}{EI} \tag{15}$$

Let $k^2 = \frac{F}{EI}$, and substitute it into Eq. (15):

$$\frac{\mathrm{d}^2\omega}{\mathrm{d}x^2} + k^2\omega = -\frac{qk^2}{2F}\left(x^2 - lx + \frac{l^2}{6}\right) \tag{16}$$

Equation (16) is a second-order non-homogeneous differential equation with constant coefficients, and the general solution of the associated homogeneous equation $\frac{\mathrm{d}^2\omega}{\mathrm{d}x^2} + k^2\omega = 0$ is:

$$\omega_1 = A\cos kx + B\sin kx \tag{17}$$

where A and B are undetermined constants.

The particular solution corresponding to the non-homogeneous term $-\frac{qk^2}{2F}\left(x^2 - lx + \frac{l^2}{6}\right)$ of Eq. (16) is:

$$\omega_2 = \frac{q}{2F}\left(-x^2 + lx - \frac{l^2}{6} + \frac{2}{k^2}\right) \tag{18}$$

Therefore, the general solution of Eq. (16) is:

$$\omega = \omega_1 + \omega_2 = A\cos kx + B\sin kx + \frac{q}{2F}\left(-x^2 + lx - \frac{l^2}{6} + \frac{2}{k^2}\right) \tag{19}$$

Based on the boundary conditions: $\omega(x=0)=0$, $\frac{d\omega}{dx}\left(x=\frac{l}{2}\right)=0$, the two undetermined constants can be derived from Eq. (19) as:

$$\begin{cases} A = \dfrac{q}{F}\left(\dfrac{l^2}{12} - \dfrac{1}{k^2}\right) \\ B = A\tan\left(\dfrac{kl}{2}\right) = \dfrac{q}{F}\left(\dfrac{l^2}{12} - \dfrac{1}{k^2}\right)\tan\left(\dfrac{kl}{2}\right) \end{cases} \tag{20}$$

Clearly, the maximum bending stress of the roadway floor strata occurs at the middle of the roadway $x = \frac{l}{2}$, and its value is:

$$\begin{aligned} \sigma_{\max} &= \sigma\Big|_{x=\frac{l}{2}} = \frac{M(x)}{W}\Big|_{x=\frac{l}{2}} - \frac{F}{h} = \left(-\frac{ql^2}{24} + F\omega(x=\frac{l}{2})\right)\left(\frac{6}{h^2}\right) - \frac{F}{h} \\ &= \left[-\frac{ql^2}{24} + F\left(A\cos\frac{kl}{2} + B\sin\frac{kl}{2} + \frac{q}{2F}\left(\frac{l^2}{12} + \frac{2}{k^2}\right)\right)\right]\left(\frac{6}{h^2}\right) - \frac{F}{h} \\ &= -\frac{\gamma l^2}{4h} + \frac{6\gamma}{k^2 h}\left[\left(\frac{k^2l^2}{12} - 1\right)\sec\left(\frac{kl}{2}\right) + \frac{k^2l^2}{24} + 1\right] - \frac{F}{h} \end{aligned} \tag{21}$$

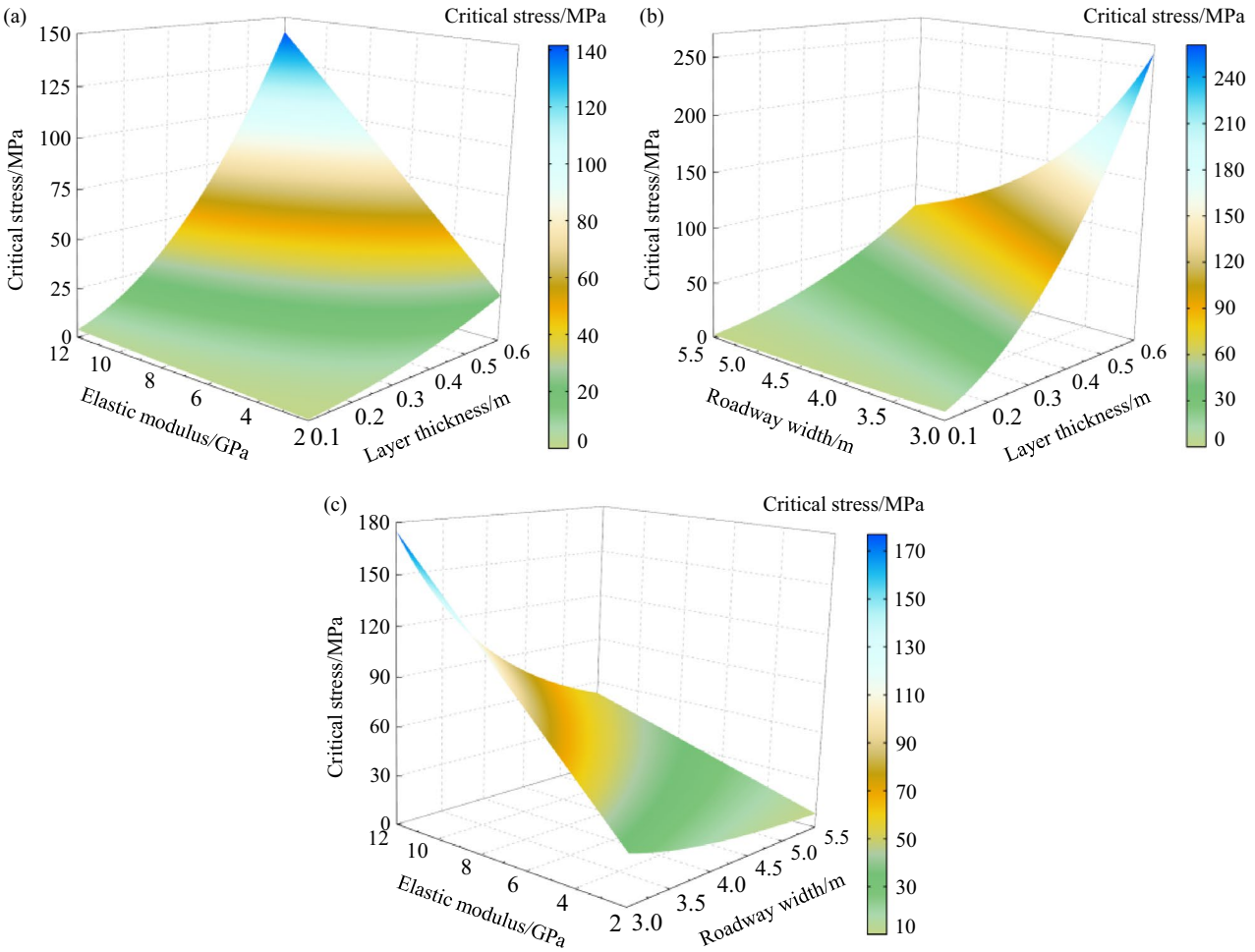

Fig. 8 Variation of the σ_{cr} with E, h, and l: **a** Variation of σ_{cr} with E and h, **b** Variation of σ_{cr} with l and h, **c** Variation of σ_{cr} with E and l

where W is the flexural section modulus, and h is the delamination layer thickness of the roadway floor strata.

When $\left(\frac{kl}{2}\right) \to \infty$ in Eq. (21), it means that the roadway floor strata fail to resist the horizontal compressive stress F, indicating the risk of buckling failure of the floor. At this point, the following conditions must be satisfied:

$$\frac{kl}{2} = n\pi + \frac{\pi}{2} = \frac{(2n+1)\pi}{2} \ (n = 0, 1, 2, \ldots) \tag{22}$$

Therefore, the critical horizontal pressure for the buckling failure of the roadway floor strata is:

$$F_{cr} = \frac{\pi^2 EI}{l^2} = \frac{\pi^2 Eh^3}{12l^2} \tag{23}$$

where F_{cr} is the critical horizontal pressure for the buckling failure of the roadway floor strata.

Assuming the width of the floor rock beam is taken as one unit along the axis of the roadway, the critical horizontal stress for the buckling failure of the roadway floor strata is:

$$\sigma_{cr} = \frac{F_{cr}}{S} = \frac{\pi^2 Eh^2}{12l^2} \tag{24}$$

where σ_{cr} is the critical horizontal stress for the buckling failure of the roadway floor strata, and S is the cross-sectional area of the floor rock beam.

Equation (24) reveals that the critical stress σ_{cr}, responsible for the buckling failure of the roadway floor strata, correlates primarily with the elastic modulus E of the floor strata, the delamination layer thickness h, and the roadway width l. To elucidate the relationship between the σ_{cr} and the variables E, h, and l, analysis using the control variate method is conducted as follows: (1) Taking l as 5 m, E as 2–12 GPa, and h as 0.1–0.6 m. (2) Taking E as 8 GPa, l as 3.0–5.5 m, and h as 0.1–0.6 m. (3) Taking h as 0.4 m, E as 2–12 GPa, and l as 3.0–5.5 m. By substituting the above parameters into Eq. (24), the variation of the σ_{cr} for the buckling failure of the roadway floor strata with the variables E, h, and l can be obtained, as shown in Fig. 8.

From Fig. 8, it can be seen that E, h, and l have a significant influence on the σ_{cr}. Specifically, σ_{cr} is positively correlated with E and h, and negatively correlated with l. By calculation, it can be found that the increase rate of σ_{cr} with the increase of E is approximately 0.33 – 14.61 MPa/GPa. The increase rate of σ_{cr} with the increase of h is approximately 4.60 – 27.61 MPa/0.1 m. The decrease rate of σ_{cr} with the increase of l is approximately -73.88 – -2.05 MPa/m. The analysis above demonstrates that the stability of the roadway floor strata can be enhanced by modifying its elastic modulus, preventing or reducing delamination, and increasing layer thickness. Practical measures include applying pre-stressed (grouted) anchor/strand bolts to the roadway floor, implementing grouting in boreholes, and reinforcing surrounding rock with steel pipe concrete. Furthermore, it is advisable to reduce the roadway width as much as possible. These measures collectively serve to increase the critical stress threshold for the buckling failure of the roadway floor strata. As a result, the roadway floor strata can withstand higher static load and disturbance dynamic load, thereby improving the stability of the roadway floor strata and preventing or reducing the incidence of coal bursts in the roadway floor.

4.2 Criteria of the coal bursts in roadway floor

Section 4.1 analyzed the stability of the roadway floor strata under horizontal static load, but the roadway floor strata are also subjected to dynamic load disturbances arising from the fracture of the thick and hard roof above the working face. Consequently, the total stress experienced by the roadway floor strata should include both static load stress and dynamic load stress. As the horizontal stress within the roadway floor strata approaches the critical stress threshold for floor strata failure, the roadway floor strata enter a critically unstable state, increasing the likelihood of coal bursts in the floor under the influence of external dynamic disturbances.

Zhao et al. (2023) proposed a method for calculating the disturbance dynamic load generated during the synchronous breakage of the overlying sub-key stratum in the fully mining stage of an adjacent working face. Employing this method and specifically considering the disturbance induced by roof breakage on the roadway floor strata in the horizontal direction, the disturbance dynamic load exerting on the roadway floor strata in the horizontal direction, generated during the synchronous breakage of the overlying sub-key stratum in the fully mining stage of the adjacent working face, can be obtained as:

$$\sigma_{xd} = 0.0645 K_d \rho V_s \left[\eta \frac{\left(q_{zI}^2 l_{zI}^5 + q_{zII}^2 l_{zII}^5 + \mathrm{L} + q_{zn}^2 l_{zn}^5\right)}{8EJ}\right]^{0.3566} L^{-\mu} \tag{25}$$

where σ_{xd} is the dynamic load stress in the horizontal direction caused by the disturbance dynamic load, K_d is the conversion coefficient for the dynamic load stress in the horizontal direction, ρ is the medium density, V_S is S-wave propagation velocity, η is the energy conversion coefficient, which can be taken as 0.1% to 1.0% (Dou et al. 2001), q_{zI}, q_{zII} … q_{zn} are overlying strata loads of the sub-key stratum I, II … n, l_{zI}, l_{zII} … l_{zn} are the periodic breakage distances of the sub-key stratum I, II … n, E is the elastic modulus of the roof strata, J is the moment of inertia, L is the distance of the vibration wave propagation caused by the breakage of the key stratum, and μ is the attenuation index, which can be taken as 1.526 (He et al. 2015).

In underground coal mines, the roadway floor strata often exhibit various defects, including joints, fractures, and failure surfaces, compromising their integrity and strength. Consequently, the effective critical stress for buckling failure of the roadway floor strata needs to be appropriately reduced from the critical horizontal stress value obtained from Eq. (24).

Based on the analysis above, the criteria for bursting instability of the roadway floor can be obtained from Eqs. (4), (24), and (25) as:

$$\begin{aligned}\sigma_{xz} =& \sigma_{xj} + \sigma_{xd} \\ =& \sum_{i=1}^{7} \Delta\sigma_{xi} + \lambda\gamma(H+y) \\ &+ 0.0645K_{d}\rho V_{s}\left[\eta\frac{\left(q_{zI}^{2}l_{zI}^{5} + q_{zII}^{2}l_{zII}^{5} + \mathrm{L} + q_{zn}^{2}l_{zn}^{5}\right)}{8EJ}\right]^{0.3566} L^{-\mu} \\ &\geq \zeta\sigma_{cr}\end{aligned} \tag{26}$$

where σ_{xz} is the total stress of the roadway floor strata in the horizontal direction, σ_{xj} is the static load stress in roadway floor strata in the horizontal direction, and ζ is the reduction coefficient for the critical horizontal stress, which is generally taken as 0.6 to 0.8, the literature (Pan et al. 2006) suggests using 0.8.

4.3 Mechanism of the coal bursts in roadway floor

In the preceding section, a comprehensive analysis of the stress distribution characteristics of GSRF was conducted. Subsequently, a model for buckling failure of the roadway floor strata was established, enabling the stability analysis of the roadway floor strata. Furthermore, the criteria for bursting instability of the roadway floor were proposed. Based on the above research, the mechanism of the coal bursts in GSRF can be derived as follows:

(1) The deep mining area of Ordos currently operates at a depth of 600 – 750 m, which implies a large foundation static load on the surrounding rock of the roadway due to the significant mining depth. During the initial production phase in this area, coal pillars with a width varying from 20 – 40 m are left behind. This practice generates high-stress concentration and energy accumulation in the local area of the coal pillar and the surrounding rock of GSR. Consequently, these conditions act as the static load source, triggering the coal bursts in GSRF.

(2) Within the deep mining area of Ordos, the coal seams are overlain by thick and hard strata, which effectively store substantial energy. A significant quantity of elastic energy is accumulated within the overlying thick and hard strata as the roof becomes suspended. Upon reaching its maximum span, the roof breaks, releasing the stored elastic energy in large quantities. This sudden release of energy manifests as a disturbance dynamic load, which acts as the primary trigger for coal bursts in GSRF.

(3) In the extraction of GSWF, the surrounding rock of GSR undergoes the combined influences of lateral static load from the adjacent gob, advanced static load from the working face, and disturbance dynamic load from the fracture of the overlying thick and hard roof. The high stress and energy are transmitted to the roadway floor through the "roof → rib → floor" pathway, leading to a concentration of high stress and an accumulation of energy within the roadway floor. Consequently, the roadway floor strata reach a critical state of instability, transforming the roadway floor into a high-risk area for coal bursts. The risk of coal bursts is amplified by the absence or the inadequacy of support provided to the roadway floor. As stress and energy accumulate due to the combined effects of dynamic and static loads, once the criteria for bursting instability of the roadway floor are met, the high stress and energy stored within the floor strata are instantaneously released. This sudden release triggers a dynamical response of the roadway floor, such as abrupt bulging and cracking, leading to coal bursts in GSRF.

5 Preventive measures for coal bursts in GSRF

The research presented in Sect. 4 identifies two primary causes of coal bursts in GSRF under thick and hard roofs: (1) Large burial depth results in substantial foundation static load on the surrounding rock. Stress and energy transmission from the roof to the roadway floor through the "roof → rib → floor" induce stress concentrations at the roadway's bottom corners. Weak support at the roadway's bottom corners, combined with dynamic load disturbances, can induce localized failures and potentially trigger roadway floor bursts; (2) The sudden fracture of the thick and hard roof generates dynamic load. These loads, transmitted through the "roof → rib → floor" pathway, create dynamic load disturbances within the surrounding rock. The combined effect of dynamic load disturbances and high static load induces horizontal stress in the floor exceeding the critical value for bursting instability, leading to coal bursts in the floor.

To mitigate dynamic load caused by thick and hard roof fracture, this paper proposes two methods: roof regional fracturing and abrasive water jet axial roof cutting. These techniques aim to mitigate or slow down dynamic load disturbances. To reduce the high static load in the surrounding

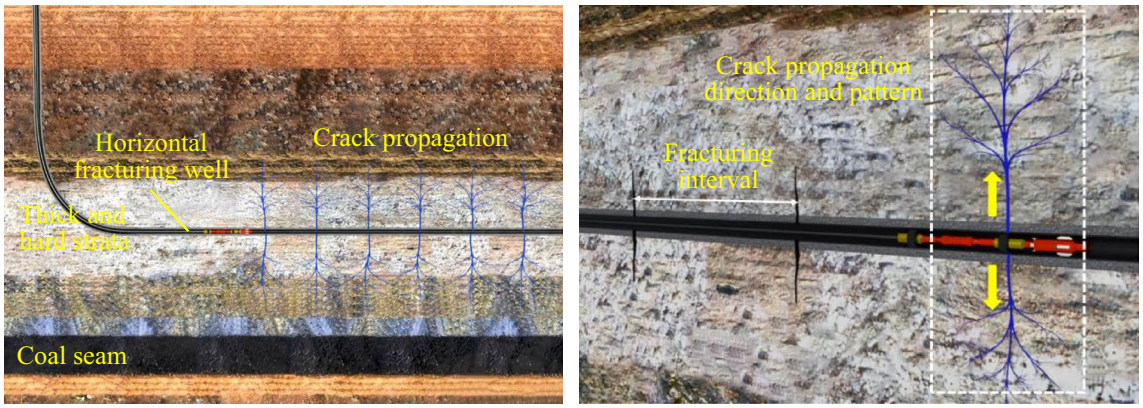

Fig. 9 Schematic diagram of surface horizontal well fracturing (modified from reference (Pan et al. 2023))

rock, the paper proposes two methods: roadway ribs hydraulic reaming of gutters, and roadway bottom corners deep hole blasting. The goal of these methods is to reduce foundation static load stress. By implementing these dynamic and static load prevention measures, the instability criteria are not met, effectively preventing coal bursts in GSRF.

5.1 Regional fracturing in thick and hard roof

To mitigate dynamic load caused by thick and hard roof fracture, surface horizontal well fracturing and underground ultra-long horizontal hole fracturing are proposed. The proposed methods aim to weaken the thick and hard roof, inducing timely collapse during mining, thereby preventing abrupt stress and energy release that generate dynamic load disturbances.

5.1.1 Surface horizontal well fracturing

Traditional hydraulic fracturing in underground coal mines faces constraints due to construction conditions, equipment, and technology. The effective range of roof fracturing typically does not exceed 50 m above the coal seam, which is ineffective for relieving pressure from high-position thick and hard strata (Yu et al. 2019). In 2020, CCTEG Coal Mining Research Institute proposed the implementation of ground horizontal well-segmented fracturing measures on the thick and hard roof. This technique aims to fracture and depressurize from the thick and hard strata above the working face, thereby mitigating the coal burst disasters in coal mines. The schematic diagram of surface horizontal well fracturing is shown in Fig. 9.

Horizontal well fracturing involves drilling from the surface into the thick and hard strata overlying the coal seam. Horizontal well fracturing is used to reduce the integrity and strength of the high-position thick and hard strata. This enables controlled fracturing and timely collapse of the thick and hard strata, preventing sudden fracture and associated dynamic load on the surrounding rock of the roadway. Consequently, this technique minimizes the risk of coal bursts on the roadway floor.

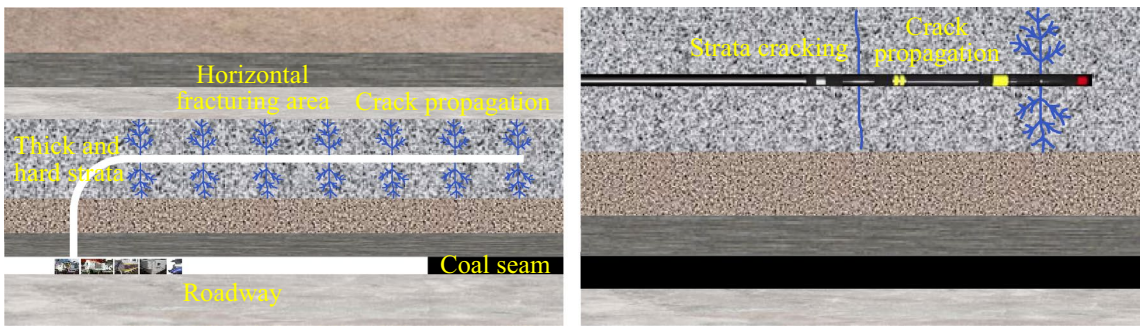

Fig. 10 Schematic diagram of underground ultra-long horizontal hole fracturing (modified from reference (Pan et al. 2022b))

5.1.2 Underground ultra-long horizontal hole fracturing

The surface horizontal well fracturing is subject to terrain and ground construction. The procedures of land acquisition, road construction, and compensation are lengthy, making the construction timeline challenging to guarantee. Additionally, the construction cost is high. Therefore, in suitable underground conditions, ultra-long horizontal hole segmented fracturing effectively fractures middle and high-position thick and hard strata, promoting timely fracture and collapse of the thick and hard roof as the working face advances. Consequently, this approach mitigates dynamic load disturbances induced by the fracturing of the thick and hard overhanging roof. It also significantly reduces the likelihood of coal bursts in roadways. The schematic diagram of underground ultra-long horizontal hole fracturing is shown in Fig. 10.

The underground ultra-long horizontal hole segmented fracturing can effectively weaken the middle and high-position thick and hard roof. It creates a network of cracks within the thick and hard strata, thereby reducing their strength. Fracturing weakens the transfer of dynamic and static loads from the overlying strata, transforming stress transfer from "hard transfer" to "soft transfer" during mining. This reduces the static load stress on the coal and rock mass. Additionally, the weakened thick and hard roof fractures and collapses in a controlled manner during mining, minimizing thick and hard roof overhang and reducing dynamic load disturbances. Consequently, the total stress exerted in roadway floor strata remains below the critical value for inducing coal bursts, effectively preventing coal bursts in the roadway caused by thick and hard roof fractures.

5.2 Abrasive water jet axial roof cutting

Abrasive water jet axial roof cutting creates parallel or perpendicular fractures within the roof, enabling controlled fracturing along predetermined cracks, thereby precisely managing the thick and hard roof. This technique mitigates dynamic load disturbances caused by abrupt fracturing of the large-scale overhanging roof, while also reducing mining-induced static load stress (Xia et al. 2020b). Generally, the abrasive water jet axial roof cutting is executed in the roadway of the previous working face to create fractures in the strike and incline directions. The schematic diagram of abrasive water jet axial roof cutting is shown in Fig. 11.

Without abrasive water jet axial roof cutting, the thick and hard roof above the working face may overhang during mining (Fig. 12a). In such cases, the load from the overhanging roof transfers to the surrounding rock and coal pillars of the GSR, resulting in increased stress. Concurrently, the abrupt fracturing of thick and hard roofs generates a dynamic load that could induce coal bursts in GSR.

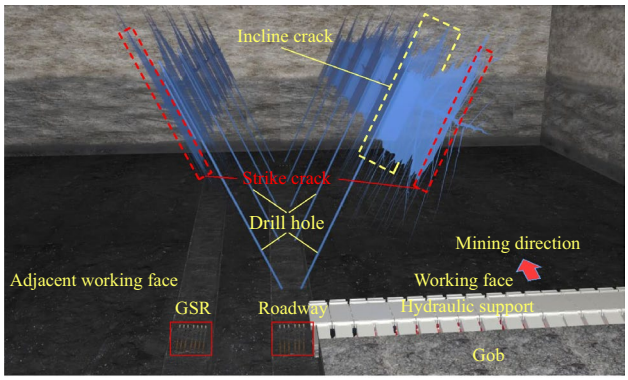

Fig. 11 Schematic diagram of abrasive water jet axial roof cutting

Upon implementing the abrasive water jet roof cutting, the roof strata fracture along predetermined fractures in both strike and incline directions, avoiding the formation of the overhanging roof (Fig. 12b). In this case, significantly reducing the lateral load of gob transfers to the surrounding rock and coal pillars of GSR. Stress on the GSR and coal pillar is reduced, and timely fracture of the roof prevents dynamic load generation. The combined loads on the surrounding rock remain below the critical value for bursting instability, preventing its occurrence in GSR.

5.3 Roadway ribs hydraulic reaming of gutters

As indicated in Sect. 4.3, coal bursts in GSRF primarily occur due to the combined dynamic and static loads of the roadway floor exceeding the critical value for floor bursting instability. The roadway ribs are the main areas where stress and energy are concentrated and accumulated. They also serve as the medium for stress and energy transfer from the roadway roof to the floor. Therefore, pressure relief in the coal body of roadway ribs can effectively reduce stress on the roadway floor, thereby mitigating the risk of coal bursts.

Conventional stress relief methods for the coal body of roadway ribs using large-diameter boreholes are influenced by borehole diameter and the extent of borehole collapse. Consequently, controlling the stress relief effect proves challenging. To address these issues, a high-pressure rotating water jet can be used to create an artificial cavity within the borehole, which exceeds the borehole's diameter, thereby broadening the pressure relief space. Field practice demonstrates that the size of the cavity after hydraulic reaming is 45–60 times that of a 150 mm borehole, with an effective pressure relief radius of 4.0 m (Xia et al. 2020a). This allows for sufficient stress relief of the coal body in roadway ribs. The schematic diagram of roadway ribs hydraulic reaming of gutters, as shown in Fig. 13.

The schematic diagram of stress distribution and transfer in the surrounding rock of the roadway before and after

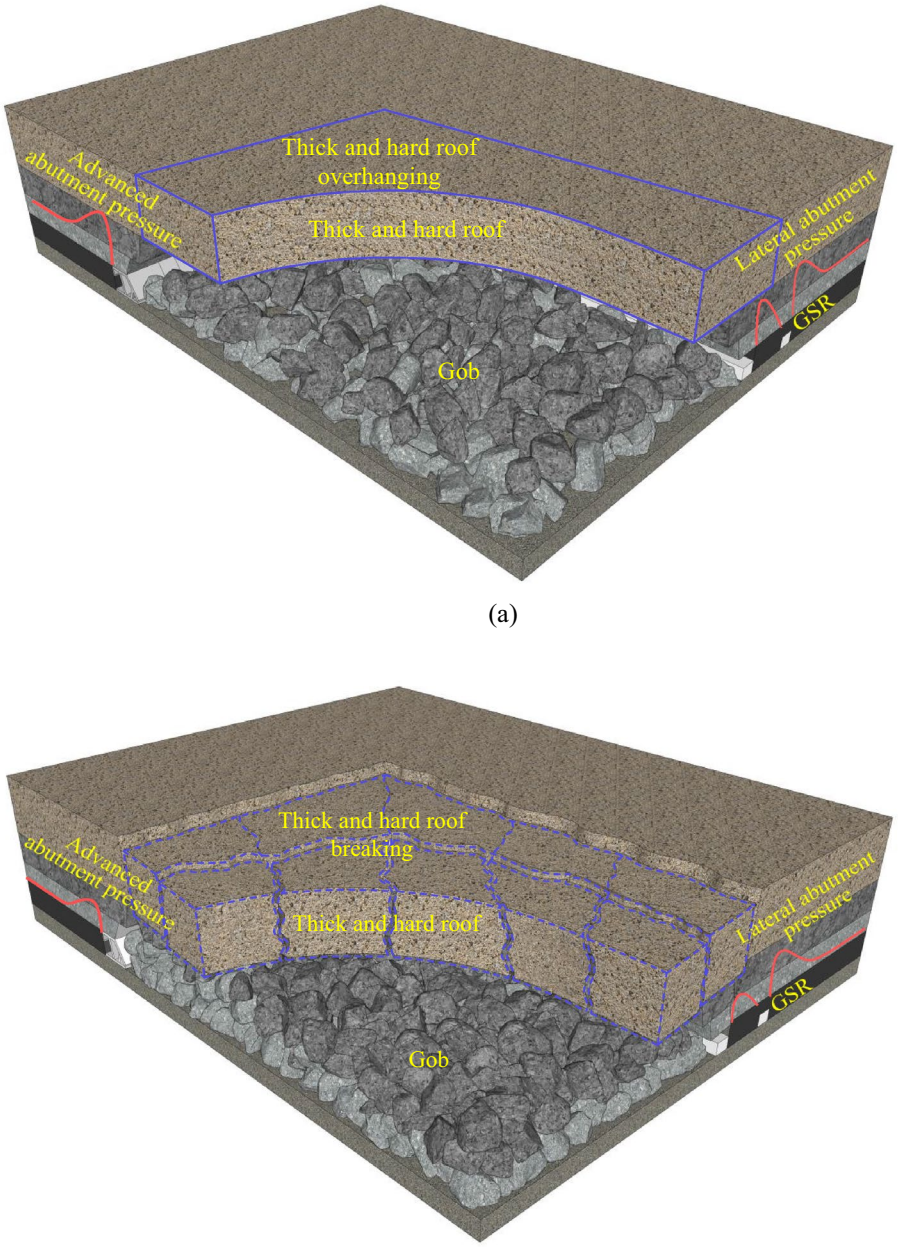

Fig. 12 Schematic diagrams of the roof structures and stress distribution in the surrounding rock of GSR before and after the implementation of abrasive water jet axial roof cutting. **a** Before the implementation of abrasive water jet axial roof cutting for stress relief; **b** After the implementation of abrasive water jet axial roof cutting for stress relief

the implementation of roadway ribs hydraulic reaming of gutters, as shown in Fig. 14. Figure 14a demonstrates that without stress relief measures in roadway ribs of GSR, stress transmitted from the roof to the floor through the coal body in roadway ribs leads to high-stress concentration and energy accumulation. Under dynamic load disturbances, when the stress and energy exceed the critical value for floor bursting instability, coal bursts occur. Figure 14b illustrates that the implementation of stress relief measures in roadway ribs of GSR significantly weakens the ability of the coal body to transmit stress and energy. This intervention effectively obstructs stress transmission from the roof to the floor through the coal body, leading to reduced stress and energy transferred to the roadway floor. This helps to avoid the formation of high-stress concentration and energy accumulation, effectively reducing the static load stress level and preventing coal bursts under dynamic load disturbances.

5.4 Roadway bottom corners deep hole blasting

Implementing roof regional fracturing or abrasive water jet axial roof cutting to treat the thick and hard roof mitigates dynamic load disturbances resulting from the fracture of the thick and hard roof. Subsequently, to further reduce the static

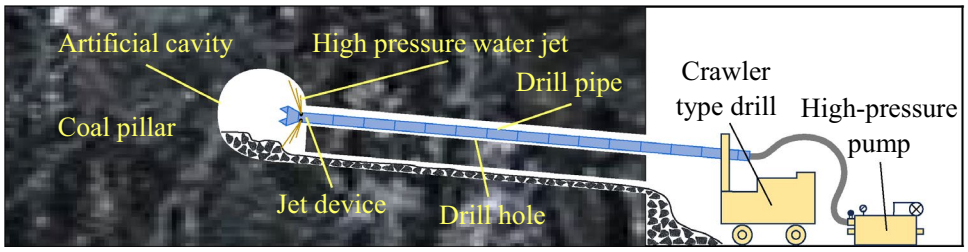

Fig. 13 Schematic diagram of roadway ribs hydraulic reaming of gutters (modified from reference (Xia et al. 2020a))

load stress on the coal body and weaken stress transfer from the roof to the floor, roadway ribs hydraulic reaming of gutters is recommended. If coal bursts still manifest despite these measures, blasting at the bottom corners of the roadway ribs can be employed to further impede the transmission of high stress and energy from the roof to the floor via the roadway ribs (bottom corners). This prevents the formation of high horizontal stress in the roadway floor, ensuring that the dynamic and static loads in roadway floor strata do not exceed the critical value for bursting instability of the roadway floor, effectively preventing coal bursts.

Stress distribution and transfer characteristics in the roadway, without bottom corners deep hole blasting, mimic those observed prior to the implementation of hydraulic reaming along the roadway ribs for stress relief (Fig. 14a). Stress transmitted from the roof to the floor via the coal body in roadway bottom corners induces high-stress concentration and energy buildup in the floor, potentially causing coal bursts under dynamic load disturbances.

Figure 15 illustrates the altered stress distribution and transfer pattern in the surrounding rock of the roadway after the implementation of deep hole blasting at the bottom corners of the roadway ribs. Deep hole blasting in the roadway bottom corners diminishes the stress and energy transmission capacity of the coal body in the bottom corners. This "blocking" effect reduces the stress and energy reaching the roadway floor. This helps to avoid the formation of high-stress concentration and energy accumulation on the roadway floor. Consequently, the static load stress level on the roadway floor is effectively reduced. Stress and energy levels remain below the critical threshold for bursting instability in the roadway floor under dynamic load disturbances, effectively preventing coal bursts.

In the above methods for preventing coal bursts in GSRF, regional fracturing can be applied to a large area of the thick and hard roof over the working face in advance. This weakens the roof, reducing the dynamic load when it breaks. The pressure and flow rate of the fracturing fluid used in surface horizontal well fracturing are greater than those in underground ultra-long hole fracturing, resulting in a better pressure relief effect. Therefore, this method is the preferred choice under suitable conditions. Abrasive water jet axial roof cutting can be used within the roadway to relieve pressure locally on the lateral roof of the working face. This promotes the breaking of the lateral roof during the mining process, avoiding the formation of stress concentration and dynamic load. It can be used for local pressure relief. Roadway ribs hydraulic reaming of gutters can relieve pressure locally on coal bodies with high static load stress, reducing the static load stress of the coal and rock mass. Roadway bottom corners deep hole blasting can be used at local positions to block the stress and energy from the surrounding rock of the roadway transferring to the floor, thereby reducing the stress on the floor strata.

The proposed methods for preventing coal bursts in GSRF are based on the mechanism of coal bursts in GSRF under the thick and hard roof. Effective control of coal bursts in GSRF necessitates the selection of appropriate prevention measures that align with the specific mining conditions, behavior characteristics of coal bursts in the floor, and prevailing underground construction conditions.

6 Conclusions

This paper takes the Hongqinghe Coal Mine as an engineering background, the stress distribution characteristics of GSRF were analyzed, and a stress calculation formula for GSRF was derived. A mechanical model of buckling failure of the roadway floor strata was established. This model facilitates the calculation of critical stress leading to buckling failure in floor strata. Based on these findings, criteria for bursting instability of GSRF were proposed. The paper further elucidates the mechanism of coal bursts in GSRF. Finally, it proposes methods to prevent coal bursts in GSRF. The primary conclusions are summarized as follows:

(1) The vertical stress increment and additional stress calculation model of GSWF was established, and the stress calculation formula for GSRF was derived. The analysis shows that the horizontal stress in the roadway floor undergoes a stress unloading state followed by a stress concentration state as the floor depth increases. As the floor depth continues to increase, it gradually approximates the in-situ stress state.
(2) A mechanical model was developed to investigate the beam-buckling failure of roadway floor strata, and a formula was derived to calculate the critical horizon-

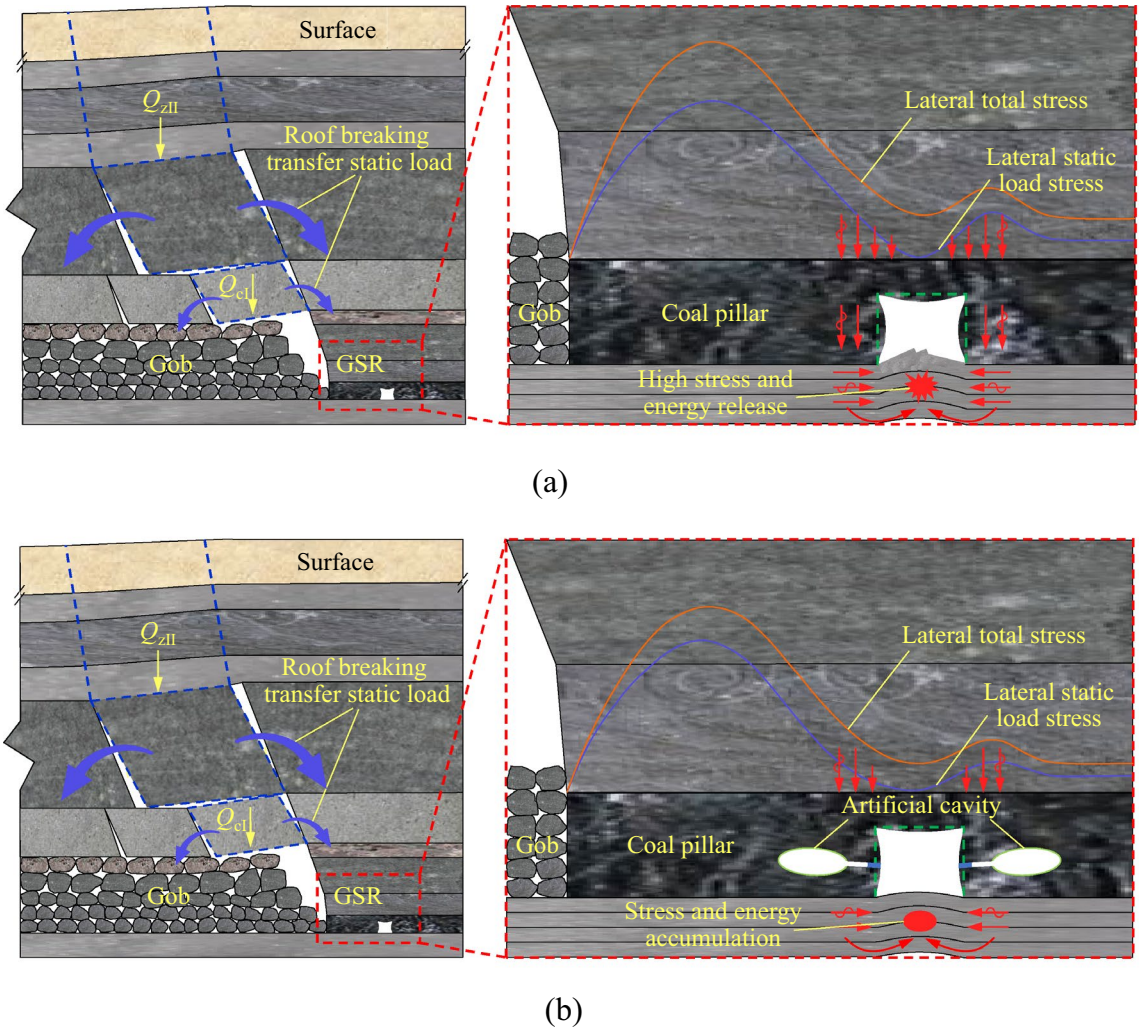

Fig. 14 Schematic diagram of distribution and transfer of stress in the surrounding rock of the roadway before and after the implementation of roadway ribs hydraulic reaming of gutters. **a** Before the implementation of abrasive water jet axial roof cutting for stress relief; **b** After the implementation of abrasive water jet axial roof cutting for stress relief

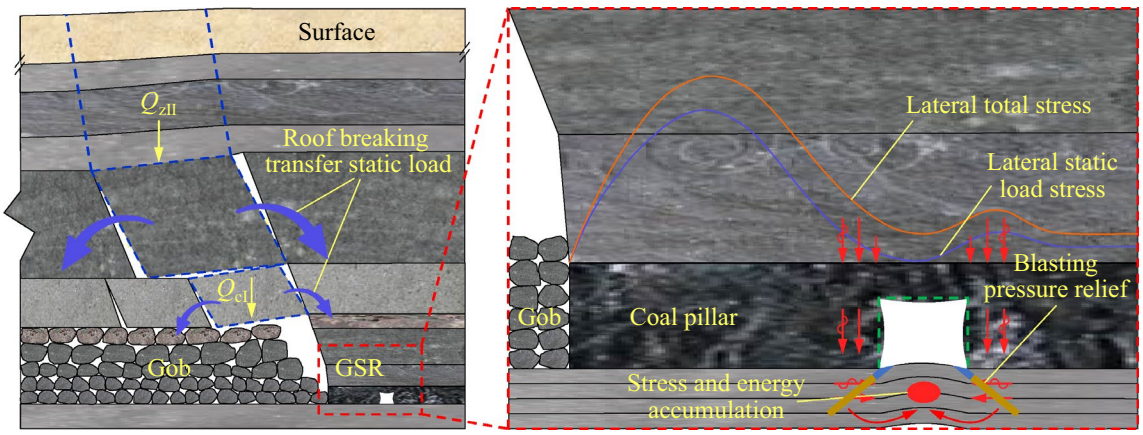

Fig. 15 Schematic diagram of distribution and transfer of stress in the surrounding rock of the roadway after the implementation of roadway bottom corners deep hole blasting

tal stress for this failure mode. The critical horizontal stress exhibits a positive correlation with the elastic modulus of the roadway floor strata and the delamination layer thickness, while it shows a negative correlation with the roadway width. Based on the dynamic and static load stress on the GSRF and its failure critical stress, criteria for bursting instability of GSRF were proposed.

(3) High static and dynamic loads are imposed on the GSR. This results in a stress concentration and energy accumulation in the roadway floor, attributable to the high stress and energy transfer through the "roof → rib → floor" pathway. Upon reaching the critical conditions for bursting instability, the accumulated stress and energy are released instantaneously, triggering dynamic responses such as abrupt cracking and bulging of the roadway floor, leading to coal bursts in GSRF.

(4) Reducing the dynamic load caused by the thick and hard roof fracturing, as well as reducing (relieving) the static load (energy) of the roadway surrounding rock is crucial for the prevention and control of coal bursts in GSRF. The regional fracturing and abrasive water jet axial roof cutting were proposed to mitigate the dynamic load. To reduce the static load of the roadway surrounding rock, roadway ribs hydraulic reaming of gutters and roadway bottom corners deep hole blasting were proposed. By implementing the above measures to control both dynamic and static loads, the criteria for bursting instability of GSRF can not be held, and the coal bursts in GSRF can be effectively controlled.

Acknowledgements The research is financially supported by the National Key Research and Development Program of China (2022YFC3004604), National Natural Science Foundation of China (U23B2093). The first author would like to thank the Prof. Yixin Zhao at China University of Mining and Technology (Beijing), China.

Author contributions Jinlong Zhou drafted the manuscript. Junfeng Pan, and Yongxue Xia provided the technical guidance. Taotao Du, Wengang Liu, and Chenyang Zhang provided writing guidance. All authors approved the final manuscript for publication.

Data availability Data will be made available on request.

Declarations

Competing interests The authors declare that they have no conflict of interest.

References

Bieniawski Z (1967) Mechanism of brittle fracture of rock. Part I-theory of the fracture process. Int J Rock Mech Min Sci 4(4):395–406. https://doi.org/10.1016/0148-9062(67)90030-7

Cao A, Zhu L, Du Z, Liu J, Wang H, Wang Y (2013) Control principle and pressure-relief technique of rock burst occurred in roadway floor. J Min Saf Eng 30(6):848–855

China National Coal Association (2024) 2023 Annual report on the development of the coal industry in China. Beijing, http://www.coalchina.org.cn

Cook N (1965) The failure of rock. Int J Rock Mech Min Sci Geomech Abstr 2(4):389–403

Cook N, Hoek E, Pretorius J (1966) Rock mechanics applied to the study of rockbursts. J South African Inst Min Metall 66(10):435–528

Dong Z, Bai J, Yan S, Wang R, Meng N, Wang G (2021) Investigation on the failure mechanism of weak floors in deep and high-stress roadway and the corresponding control technology. Minerals 11(12):1408. https://doi.org/10.3390/min11121408

Dou L, He X (2001) Theory and technology of rock burst prevention. China University of Mining and Technology Press, Xuzhou

Dou L, Lu C, Mou Z, Qin Y, Yao J (2005) Intensity weakening theory for rockburst and its application. J China Coal Soc 30(5):690–694. https://doi.org/10.3321/j.issn:0253-9993.2005.06.003

Dou L, Mu Z, Li Z, Cao A, Gong S (2014) Research progress of monitoring, forecasting, and prevention of rockburst in underground coal mining in China. Int J Coal Sci Technol 1(3):278–288. https://doi.org/10.1007/s40789-014-0044-z

Fan J, Dou L, He H, Du T, Zhang S, Gui B, Sun X (2012) Directional hydraulic fracturing to control hard-roof rockburst in coal mines. Int J Min Sci Technol 22(2):177–181. https://doi.org/10.1016/j.ijmst.2011.08.007

Fu Y, Ju W, Wu Y, He J, Jiao J (2019) Study on principle application of energy absorption and bump reduction of high impact toughness rock bolt. Coal Sci Technol 47(11):68–75. https://doi.org/10.13199/j.cnki.cst.2019.11.008

Gao R, Kuang T, Zhang Y, Zhang W, Quan C (2021) Controlling mine pressure by subjecting high-level hard rock strata to ground fracturing. Int J Coal Sci Technol 8(6):1336–1350. https://doi.org/10.1007/s40789-020-00405-1

Gong F, Luo S, Jiang Q, Xu L (2022) Theoretical verification of the rationality of strain energy storage index as rockburst criterion based on linear energy storage law. J Rock Mech Geotech Eng 14(6):1737–1746. https://doi.org/10.1016/j.jrmge.2021.12.015

Guo C, Han J (2023) Research on energy absorbing components of ZQL hydraulic support. J Brazilian Soc Mech Sci Eng 45(3):1–9. https://doi.org/10.1007/s40430-022-03999-6

Guo D, Kang X, Lu Z, Chen Q (2021) Mechanism and control of roadway floor rock burst induced by high horizontal stress. Shock Vibrat 2021(1):6745930. https://doi.org/10.1155/2021/6745930

He M, Wang Q (2023) Rock dynamics in deep mining. Int J Min Sci Technol 33(9):1065–1082. https://doi.org/10.1016/j.ijmst.2023.07.006

He H, Dou L, Fan J, Du T, Sun X (2012) Deep-hole directional fracturing of thick hard roof for rockburst prevention. Tunn Undergr Sp Technol 32:34–43. https://doi.org/10.1016/j.tust.2012.05.002

He J, Dou L, Cai W, Li Z, Ding Y (2015) In situ test study of characteristics of coal mining dynamic load. Shock Vibrat 2015(1):121053. https://doi.org/10.1155/2015/121053

He J, Dou L, Gong S, Li J, Ma Z (2017) Rock burst assessment and prediction by dynamic and static stress analysis based on microseismic monitoring. Int J Rock Mech Min Sci 93:46–53. https://doi.org/10.1016/j.ijrmms.2017.01.005

Hua A (1983) The effect of coal extraction on seam floor. J China Coal Soc 3:36–45. https://doi.org/10.13225/j.cnki.jccs.1983.03.004

Huang B, Liu J, Zhang Q (2018) The reasonable breaking location of overhanging hard roof for directional hydraulic fracturing to control strong strata behaviors of gob-side entry. Int J Rock Mech Min Sci 103:1–11. https://doi.org/10.1016/j.ijrmms.2018.01.013

Hudson J, Crouch S, Fairhurst C (1972) Soft, stiff and servo-controlled testing machines: a review with reference to rock failure. Eng Geol 6(3):155–189. https://doi.org/10.1016/0013-7952(72)90001-4

Kang H (2008) Analysis on types and interaction of stress fields in underground coal mines. J China Coal Soc 33(12):1329–1335. https://doi.org/10.13225/j.cnki.jccs.2008.12.009

Kang H, Yang J, Gao F, Li J (2020) Experimental study on the mechanical behavior of rock bolts subjected to complex static and dynamic loads. Rock Mech Rock Eng 53(11):4993–5004. https://doi.org/10.1007/s00603-020-02205-0

Kang H, Jiang P, Feng Y, Gao F, Zhang Z, Liu X (2022) Application of large-scale hydraulic fracturing for reducing mining-induced stress and microseismic events: a comprehensive case study. Rock Mech Rock Eng 56(2):1399–1413. https://doi.org/10.1007/s00603-022-03061-w

Li Y (1985) Rockburst mechanism and its preliminary application. J China Inst Min Technol 3:42–48

Li Z, Dou L, Wang G, Cai W, He J, Ding Y (2015) Risk evaluation of rock burst through theory of static and dynamic stresses superposition. J Cent South Univ 22(2):676–683. https://doi.org/10.1007/s11771-015-2570-2

Linkov A (1996) Rockbursts and the instability of rock masses. Int J Rock Mech Min Sci Geomech 33(7):727–732. https://doi.org/10.1016/0148-9062(96)00021-6

Liu Y, Zhao H, Liu S, Sun W (2022) Asymmetric damage mechanism of floor roadway based on zonal damage characteristics of longwall panel floor: a case study. Nat Hazards 114(1):1015–1041. https://doi.org/10.1007/s11069-022-05421-9

Lou J, Gao F, Li J, Yuan G, Sharifzadeh M (2023) Effect of dynamic loading conditions on the dynamic performance of MP1 energy-absorbing rockbolts: insight from laboratory drop test. Int J Min Sci Technol 33(2):215–231. https://doi.org/10.1016/j.ijmst.2022.09.023

Ma B, Tai Y, Li Y, Xia H, Meng X (2023) Investigation of the process of perforating hard roof in an innovative technology of directional roof-cutting by composite blasting. Energy Sci Eng 11(7):2585–2600. https://doi.org/10.1002/ese3.1475

Mu Z, Liu G, Yang J, Zhao Q, Javed A, Gong S, Cao J (2019) Theoretical and numerical investigations of floor dynamic rupture: a case study in Zhaolou Coal Mine, China. Saf Sci 114:1–11. https://doi.org/10.1016/j.ssci.2018.12.016

Pan Y (2018) Disturbance response instability theory of rockburst in coal mine. J China Coal Soc 43(8):2091–2098. https://doi.org/10.13225/j.cnki.jccs.2018.0604

Pan Y, Wang A (2023) Geohazard mechanics disturbance response instability theory of rock bursts in coal mines and its application. Geohazard Mech 1(1):1–17. https://doi.org/10.1016/j.ghm.2022.12.002

Pan L, Zhang L, Liu X (2006) Practical Techniques for Predicting and Preventing of Coal Burst. China University of Mining and Technology Press, Xuzhou

Pan J, Ning Y, Mao D, Lan H, Du T, Peng Y (2012) Theory of rockburst start-up during coal mining. Chinese J Rock Mech Eng 31(3):586–596. https://doi.org/10.1007/s11783-011-0280-z

Pan Y, Qi Q, Wang A, Xiao Y, Chen J, Lv X, Xu L, Dai L (2020) Theory and technology of three levels support in bump-prone roadway. J China Coal Soc 45(5):1585–1594. https://doi.org/10.13225/j.cnki.jccs.DY20.0261

Pan C, Xia B, Zuo Y, Yu B, Ou C (2022a) Mechanism and control technology of strong ground pressure behaviour induced by high-position hard roofs in extra-thick coal seam mining. Int J Min Sci Technol 32(3):499–511. https://doi.org/10.1016/j.ijmst.2022.01.006

Pan J, Du T, Gao J, Xie F (2022b) Mechanism and prevention of rockburst in deep multipillar gob-side entry. Lithosphere. https://doi.org/10.2113/2022/1509697

Pan J, Lu C, Ma X, Xia Y, Xie F, Xu G, Dou G, Lv D, Sun X, Ma W (2023) System and application of regional fracking of coal seam roof on and under the ground to prevent rockburst. Coal Sci Technol 51(2):106–115. https://doi.org/10.13199/j.cnki.cst.2022-0903

Qi Q, Liu T, Shi Y (1995) Mechanism of fraction sliding disability of rock burst. Gr Press Strat Control 12(3):174–177

Qian M, Shi P, Xu J (2010) Mine Pressure and Ground Control. China University of Mining and Technology Press, Xuzhou

Shan R, Li Z, Wang C, Wei Y, Tong X, Liu S, Shan Z (2021) Study on the distribution characteristics of stress deviator in the surrounding rock when mining closely spaced coal seams. Environ Earth Sci 80(17):1–18. https://doi.org/10.1007/s12665-021-09891-1

Shan R, Li Z, Wang C, Meng C, Wei Y, Li Y, Tong X, Liu D (2022) Study on distortion energy and stability of gob floor based on stress deviator field. Energy Sci Eng 10(8):2756–2771. https://doi.org/10.1002/ese3.1165

Suchowerska A, Merifield R, Carter J (2013) Vertical stress changes in multi-seam mining under supercritical longwall panels. Int J Rock Mech Min Sci 61:306–320. https://doi.org/10.1016/j.ijrmms.2013.02.009

Suchowerska A, Carter J, Merifield R (2014) Horizontal stress under supercritical longwall panels. Int J Rock Mech Min Sci 70:240–251. https://doi.org/10.1016/j.ijrmms.2014.03.009

Sun X, Fang X, Guan L (2009) Mechanics of Materials. Higher Education Press, Beijing

Tang Z, Zuo W, Lv J, Yu M, Wu Z (2023) Study on factors influencing mechanical properties of energy absorbers for hydraulic support in rockburst roadway. Int J Adv Manuf Technol. https://doi.org/10.1007/s00170-023-10852-0

Wang Q, Jiang B, Xu S, He M, Jiang Z, Li S, Wei H, Xiao Y (2022a) Roof-cutting and energy-absorbing method for dynamic disaster control in deep coal mine. Int J Rock Mech Min Sci 158:105186. https://doi.org/10.1016/j.ijrmms.2022.105186

Wang Q, Xu S, Xin Z, He M, Wei H, Jiang B (2022b) Mechanical properties and field application of constant resistance energy-absorbing anchor cable. Tunn Undergr Sp Technol 125:104526. https://doi.org/10.1016/j.tust.2022.104526

Wang H, Wang J, Elmo D, He M, Ma Z, Gao C (2023a) Ground response mechanism of entries and control methods induced by hard roof in longwall top coal caving panel. Eng Fail Anal 144:106940. https://doi.org/10.1016/j.engfailanal.2022.106940

Wang Q, Jiang Z, Jiang B, He M, Yang J, Xue H (2023b) Ground control method of using roof cutting pressure release and energy-absorbing reinforcement for roadway with extra-thick hard roof. Rock Mech Rock Eng 56(10):7197–7215. https://doi.org/10.1007/s00603-023-03461-6

Wawersik W, Fairhurst C (1970) A study of brittle rock fracture in laboratory compression experiments. Int J Rock Mech Min Sci 7(5):561–575. https://doi.org/10.1016/0148-9062(70)90007-0

Wu K, Zou J, Jiao Y, He S, Wang G (2023) Insight and effectiveness of working-face deep-hole blasting for prevention of strong seismicity induced by deep coal mining. Rock Mech Rock Eng. https://doi.org/10.1007/s00603-023-03516-8

Xia Y, Ju W, Su S, Lu Q, Ding G, Su B, Chen Z (2020a) Experimental study on hydraulic reaming of gutters in coal seam with impact pressure. J Min Strat Control Eng 2(1):013022. https://doi.org/10.13532/j.jmsce.cn10-1638/td.2020.01.009

Xia Y, Lu C, Yang G, Su S, Pang L, Ding G, Su B (2020b) Experimental study on axial fracture cutting and fracturing of abrasive jet in hard roof hole. J Min Strat Control Eng 2(3):033522. https://doi.org/10.13532/j.jmsce.cn10-1638/td.20200522.001

Xu Z (2018) Concise Tutorial on Elasticity. Higher Education Press, Beijing

Yang R, Zhu Y, Li Y, Li W, Xiao B (2020) Stability analysis and control strategy of weakly cemented layered floor in mining affected roadway. J China Coal Soc 45(7):2667–2680. https://doi.org/10.13225/j.cnki.jccs.2020.0123

Yang J, Fu Q, Gao Y, Li C, Chang X, Wu X (2023) A novel method of roadway floor deformation control by deep-hole directional tension blasting-a case study. Mining, Metall Explor 40(4):1121–1140. https://doi.org/10.1007/s42461-023-00790-6

Yu B, Gao R, Kuang T, Huo B, Meng X (2019) Engineering study on fracturing high-level hard rock strata by ground hydraulic action. Tunn Undergr Sp Technol 86:156–164. https://doi.org/10.1016/j.tust.2019.01.019

Zhang X, Hu J, Xue H, Mao W, Gao Y, Yang J, He M (2020) Innovative approach based on roof cutting by energy-gathering blasting for protecting roadways in coal mines. Tunn Undergr Sp Technol 99:103387. https://doi.org/10.1016/j.tust.2020.103387

Zhang F, Wang X, Bai J, Wu W, Wu B, Wang G (2022) Fixed-length roof cutting with vertical hydraulic fracture based on the stress shadow effect: a case study. Int J Min Sci Technol 32(2):295–308. https://doi.org/10.1016/j.ijmst.2021.09.007

Zhao Z, Ma N, Guo X, Zhao X, Xia Y, Ma Z (2016) Mechanism conjecture of butterfly rock burst in coal seam roadway. J China Coal Soc 41(11):2689–2697. https://doi.org/10.13225/j.cnki.jccs.2016.0786

Zhao Y, Zhou J, Zhang C, Liu B, Ling C, Liu W, Han C (2023) Failure mechanism of gob-side roadway in deep coal mining in the Xinjie mining area : theoretical analysis and numerical simulation. J Cent South Univ 30(5):1631–1648. https://doi.org/10.1007/s11771-023-5315-7

Zhou C, Huang C, Chen Y, Zhang W, Wang L (2023) Performance of a novel resistant rock bolt with periodic energy absorption and release: theory and experiment. Acta Geotech. https://doi.org/10.1007/s11440-023-01943-z